THE ASTROPHYSICAL JOURNAL, 503:857–876, 1998 August 20
© 1998. The American Astronomical Society. All rights reserved. Printed in U.S.A.

THERMAL EVOLUTION OF THE ENVELOPE OF SN 1987A

MARTIJN DE KOOL,[1] HONGWEI LI, AND RICHARD MCCRAY
Joint Institute for Laboratory Astrophysics, University of Colorado, and National Institute of Standards and Technology, Boulder, CO 80309-0440;
martijn@maths.anu.edu.au, hongwei@jila02.colorado.edu, dick@jila.colorado.edu
Received 1997 October 14; accepted 1998 March 27

ABSTRACT

We model the heating and cooling processes in the hydrogen- and helium-rich zones of the envelope of SN 1987A from $t = 200$ to 1200 days after outburst and use these results to calculate the light curves of the most prominent emission lines. For the first 600 days, heating and cooling processes are in equilibrium. The main heating mechanism is direct heat deposition by nonthermal electrons, and the main cooling mechanism is collisional excitation of trace elements such as Ca II, Fe II, and C I, followed by the emission of a line photon. After 600 days adiabatic cooling becomes important, and the cooling and heating rates are no longer in equilibrium. Dust, formed in the Fe/Co/Ni zone after $t \sim 400$ days, plays an important role in the formation of the emission lines. It both modifies the internal UV radiation field that excites the ions and reduces the escaping line fluxes by extinction. The pseudocontinuum opacity in the envelope due to the many absorption lines of metals, which we model crudely by a simple power law, is also important for the emerging spectrum.

Our results for the temperature evolution do not depend strongly on our assumptions. We find that the temperatures of the hydrogen and helium zones evolve from $T \approx 6000$ K at $t = 200$ days to $T \approx 1000$ K at $t = 1200$ days. The ionized fraction of hydrogen evolves from $x_{\rm H} \approx 6 \times 10^{-3}$ at $t = 200$ days to $x_{\rm H} \approx 3 \times 10^{-4}$ at $t = 1200$ days. With abundances determined from observations of the circumstellar ring, the model can account for the light curves of most strong emission lines of H I, He I, Ca II, and Fe II, but some discrepancies remain. Especially interesting is the Hβ light curve, which exhibits a clear plateau when Hβ is still optically thick, but Paα is already optically thin. In all our models this phase appears to occur later than in the observations.

For $t \gtrsim 800$ days, the infrared emission lines of Fe II are produced mainly by primordial iron in the H/He envelope, not by newly synthesized iron. The fluxes of C I and O I lines that our model predicts are much higher than observed, and they may require a significant adjustment in abundance or mass of the different composition zones to make them agree with observations. Our models also indicate that the total helium mass in the core of the remnant ($v < 2500$ km s^{-1}) must lie in the range 2–5 $M_\odot$. The hydrogen mass in the core is less well constrained, because the hydrogen line strength does not vary much as long as most of the nonthermal energy is deposited in hydrogen. The ratio of the fluxes of the Brγ and the He I 2.058 μm lines is slightly more sensitive, and it indicates a helium mass–to–hydrogen mass ratio $\sim$ 1:2.

Subject headings: line: formation — stars: abundances — supernovae: individual (SN 1987A)

1. INTRODUCTION

The thermal evolution of a supernova envelope can be deduced in two ways. If adequate data are available, as is the case with SN 1987A, the most reliable method is to infer the temperature directly from the observed intensities and ratios of emission lines (e.g., Moseley et al. 1989; Haas et al. 1990; Li & McCray 1992, 1993; Colgan et al. 1993). Such studies have shown that the emitting region of the envelope of SN 1987A must consist of zones having distinct chemical compositions and thermal histories (McCray 1996; Fransson, Houck, & Kozma 1996). It is also possible to follow the temperature evolution of each zone theoretically by considering all heating and cooling processes. In the case of SN 1987A, such a model could verify that we have identified the main atomic processes determining the temperature evolution. If we succeed in doing so, we can with greater confidence interpret the nebular spectra of other supernovae, for which we lack sufficient spectral coverage to infer the temperature evolution directly from observations.

There have been several attempts to model the temperature evolution of supernova envelopes during the nebular phase, beginning with Axelrod's (1980) pioneering models of SNIa's. Soon after the appearance of SN 1987A, Fransson & Chevalier (1987), Colgan & Hollenbach (1988), and Swartz, Harkness, & Wheeler (1987) developed models to interpret and predict the evolution of its spectrum; but these early models did not incorporate sufficient information to account in detail for the evolution of the actual observed spectrum. The models presented here use a more accurate description of the way the gamma rays from radioactive decay deposit their energy, include more detailed atomic physics, and treat the radiation field in the envelope in considerably more detail than previous work. The temperature evolution of SN 1987A has also been modeled independently by Kozma & Fransson (1998a, 1998b; hereafter KF), and we will occasionally compare our results to theirs.

Li, McCray, & Sunyaev (1993) developed a detailed model for the thermal evolution and line emission from the zones containing newly synthesized iron, cobalt, and nickel. Their model was fairly successful in accounting for the early ($t \lesssim 600$ days) light curves of many infrared emission lines

[1] Currently at the ANUATC, John Dedman Building, ANU ACT 0200, Australia.

from these elements. It also demonstrated the remarkable fact that the Fe/Co/Ni zones must occupy $\sim 50\%$ of the line-emitting region, evidently because the clumps containing these elements expanded during the first few weeks after the explosion as a result of local heating from the decay of ^{56}Ni (Basko 1994). Except for the volume filling factor of Fe/Co/Ni resulting from this early expansion, the model by Li et al. (1993) has essentially no free parameters. The model failed to account for the light curves of the emission lines of Fe II for $t \gtrsim 600$ days, however.

For $t \gtrsim 2$ yr after outburst, most of the bright emission lines in the nebular spectrum of SN 1987A must come from the hydrogen and helium zones. That is true because the gamma rays from the newly synthesized ^{56}Co and ^{57}Co illuminate the emitting region roughly uniformly. Since the hydrogen and helium zones must comprise most of the mass of the emitting region, these elements must absorb and reradiate most of the gamma-ray luminosity. Therefore, to understand the emission-line spectrum of SN 1987A, it is essential to model the emission from the H and He zones. Recombination lines are ineffective in removing the heat deposited in the hydrogen envelope by the gamma rays because the envelope is too cool for excitation or ionization by thermal electrons (they are excited and ionized almost entirely by nonthermal electrons). The hydrogen zone must cool by radiating emission lines of other elements. The main cooling lines are expected to be [Ca II] λ7300 and Ca II λ8600, which, after Hα, are the strongest emission lines seen in the spectrum of SN 1987A. In a study of these lines, Li & McCray (1993) concluded that they must be emitted by calcium that is microscopically mixed with hydrogen in primordial (LMC) abundance ratio and not by newly synthesized calcium. Moreover, unlike the hydrogen recombination lines, the luminosities of the Ca II emission lines are sensitive to the temperature of the emitting region. Therefore, Li & McCray (1993) were able to infer the temperature evolution of the hydrogen zone from the observed light curves of the Ca II lines.

We have several motives in developing a model for the thermal evolution of the hydrogen and helium zones in SN 1987A.

1. We want to be sure that we understand the physics underlying the formation of the spectrum.
2. We want to check if the masses and abundances of the H and He zones that have been calculated in explosion models are consistent with the observed emission-line fluxes.
3. We want to be able to determine the temperature at late times ($t \gtrsim 800$ days) when the Ca II line strengths became unreliable temperature diagnostics.

As Li & McCray (1996) have shown, the ultraviolet opacity of the hydrogen and helium zones, which is dominated by many thousands of resonance transitions of iron group elements, is sensitive to temperature. As the envelope cools down, radiation begins to escape through "windows" in the ultraviolet spectrum. With spectrometers aboard the *Hubble Space Telescope* (*HST*), we have seen that an increasing fraction of the luminosity of SN 1987A has emerged through such windows. Therefore, we need a more detailed understanding of the thermal evolution of the gas to interpret these observations.

In this paper we calculate the evolution of the envelope from 200 to 1200 days after the explosion. The starting time is set by the condition that the optical depth for the gamma rays not be too high, so that radiative transfer effects in the gamma rays are not important, and we end our calculation when the temperature has become so low that molecular processes, which we do not model, are expected to become important. The paper is arranged as follows. In § 2 we give an overview of the basic properties of our model of the expanding envelope of SN 1987A. Readers not interested in the details of our calculations can skip §§ 3–7, which are rather technical, and proceed directly to § 8, containing our results. For those interested in all details, § 3 contains a description of the energy deposition (ionization, excitation, and heating) by gamma rays in the envelope. In § 4 we review the physical processes and equations determining the emission-line spectrum. In § 5 we discuss the atomic processes that control the temperature of the gas. In § 6 we describe the interactions of matter and radiation with the dust. In § 7 we briefly describe our numerical method. In § 8 we present the results of our model calculations and compare them to observations. Finally, in § 9 we summarize the main points that we have learned from this study, and we discuss the limitations of our approximations.

2. GEOMETRY AND COMPOSITION OF THE MODEL

We consider a uniform, freely expanding envelope of SN 1987A and confine our attention to the the main emitting region ($v \le v_{\max} = 2500$ km s^{-1}). Calculations of the early emergence of X-rays and gamma rays from this region (e.g., Burrows & Van Riper 1995) indicate that it must have net mass $M > 5\,M_\odot$, and more likely, $M \approx 10\,M_\odot$.

We assume that this region contains "clumps" of different elemental composition (H-rich, He-rich, O-rich, Fe-rich, etc.) that are mixed macroscopically but not microscopically throughout the region. Here we model the hydrogen and helium clumps, which we assume to have uniform density and to be illuminated by a uniform flux of gamma rays (§ 3).

According to Li et al. (1993), Fe/Co/Ni clumps should occupy approximately 50% of the inner emitting volume of the envelope. Since the mass $M_{\rm He}$ of helium-rich gas is less than the mass $M_{\rm H}$ of the hydrogen, we assume that 30% of the main emitting volume is occupied by hydrogen, 10% by helium-rich clumps, and 10%, by other components (oxygen, etc.) in order to calculate the density of the hydrogen and helium zones.

The H-rich and He-rich clumps comprise most of the mass of the emitting region (the remaining part of $\sim 1\,M_\odot$ being composed primarily of O, Si, Fe, etc.). Trace elements, such as carbon, oxygen, calcium, iron, cobalt, and nickel play a crucial role in determining the thermal evolution and line emission from the hydrogen and helium zones of SN 1987A. We assume that these metals have net abundances of 0.3 times the solar values (Anders & Grevesse 1989), as observed in LMC planetary nebulae (Dufour 1984; Dopita & Meatherington 1991). Lundqvist & Fransson (1996) also find that the circumstellar ring material around SN 1987A has a metal abundance of about 0.3 times solar. However, the distribution among C, N, and O appears to be different from solar, and they derive ratios of N/C ~ 5.0 and N/O ~ 1.1. Since the circumstellar matter is likely to consist of expelled envelope material, we adopt these abundances for our hydrogen zone.

Following S. Woosley (1994, private communication) and Li & McCray (1995), we divide the helium-rich gas into two

distinct composition zones: a carbon-oxygen–rich zone with He:C:O = 1:2.2 × 10^{-2}:2.1 × 10^{-3} and a carbon-oxygen–poor zone with He:C:O = 1:9.6 × 10^{-4}:1.1 × 10^{-5}. We assume that the other metals in the helium zones have the same relative abundances as in the hydrogen-rich zone. Oxygen in the H/He envelope is mostly neutral, while most metals are singly ionized owing to exothermic charge transfer with ionized hydrogen.

The masses contained in the H-rich and He-rich zones in the envelope of SN 1987A have not been well determined, and one of the goals of this paper is to constrain them. We will present the results of our calculation for one "standard" set of masses and indicate how the results depend on changing these where appropriate. The standard model has 6 $M_\odot$ of hydrogen and 2 $M_\odot$ of helium in the hydrogen zone, and 1 $M_\odot$ of helium in the helium zones. The He zone mass is distributed over the carbon-rich He zone 1 and the carbon-poor He zone 2 in a ratio 1.96:1.26 (S. Woosley 1994, private communication).

The next few sections (§§ 3–7) contain the details of our input physics, and the reader mainly interested in our results should now proceed to § 8.

3. GAMMA-RAY ENERGY DEPOSITION

For $t \lesssim 3$ yr after outburst, the main energy sources in the envelope of SN 1987A are the radioactive decays of ^{56}Co and ^{57}Co, which produce gamma rays, positrons, and internal conversion (IC) electrons. The positrons and IC electrons deposit their energy locally in Fe/Co/Ni clumps if the magnetic field exceeds about 10^{-12} G. With $M(^{56}\mathrm{Co}) = 0.075\ M_\odot$ and $M(^{57}\mathrm{Co}) = 1.5[^{57}\mathrm{Fe}/^{56}\mathrm{Fe}]_\odot\ M(^{56}\mathrm{Co}) = 0.0027\ M_\odot$, the gamma-ray energy release rates are (Woosley, Pinto, & Hartmann 1989)

$$L^\gamma(^{56}\mathrm{Co}) = 9.54 \times 10^{41} \exp\left(-\frac{t}{t_{56}}\right) \text{ ergs s}^{-1}\,, \quad (1)$$

$$L^\gamma(^{57}\mathrm{Co}) = 3.71 \times 10^{38} \exp\left(-\frac{t}{t_{57}}\right) \text{ ergs s}^{-1}\,, \quad (2)$$

where $t_{56} = 111.3$ days and $t_{57} = 391.2$ days. In all our models we have kept $M(^{56}\mathrm{Co})$ and $M(^{57}\mathrm{Co})$ fixed at the values above. The total gamma-ray energy deposited in the envelope is

$$L^\gamma_{\rm dep} = L^\gamma_{\rm dep}(56) + L^\gamma_{\rm dep}(57)\,, \quad (3)$$

where

$$L^\gamma_{\rm dep}(56) = f^\gamma(\kappa_{56}) L^\gamma(^{56}\mathrm{Co})\,, \quad (4)$$

$$L^\gamma_{\rm dep}(57) = f^\gamma(\kappa_{57}) L^\gamma(^{57}\mathrm{Co})\,, \quad (5)$$

and f^γs are the fractions of the gamma-ray luminosity deposited in the envelope. Following Woosley et al. (1989), we write

$$f^\gamma(\kappa) = 1 - \exp\left[-\kappa\phi_0\left(\frac{t_0}{t}\right)^2\right], \quad (6)$$

where $\phi_0 = 7 \times 10^4 (M_{\rm env}/10\ M_\odot)$ g cm^{-2} is the column density of the envelope at $t = t_0$, $t_0 = 10^6$s, $\kappa_{56} = 0.033$ cm^2 g^{-1} for ^{56}Co, and $\kappa_{57} = 2.4\kappa_{56}$ for ^{57}Co. The corresponding optical depths of the envelope for the gamma rays are

$$\tau_{56} = 2.3\left(\frac{t}{1\text{ yr}}\right)^{-2}\,, \quad (7)$$

$$\tau_{57} = 5.5\left(\frac{t}{1\text{ yr}}\right)^{-2}\,. \quad (8)$$

For the time interval that we consider ($t > 200$ days), most of the gamma-ray luminosity deposited in the envelope is absorbed by the substrate (regions composed primarily of hydrogen, helium, oxygen, etc.), apart from a small fraction that is absorbed in the Fe/Co/Ni clumps. We model the absorption in the Fe/Co/Ni clumps as described by Li et al. (1993). The correction for energy deposited in the Fe/Co/Ni clumps never exceeds more than a few percent, and it is thus not important for the evolution of the H and He zones.

Our calculations do not include a detailed model of the transport of the gamma-ray photons, which could influence the results for times $\lesssim 500$ days, before the envelope becomes optically thin. We assume that the envelope is illuminated uniformly by gamma rays, corresponding to a geometry in which many Fe/Co/Ni clumps are distributed throughout the envelope, as suggested by Li et al. (1993). If so, the energy deposited in any element owing to Compton scattering should be proportional to the mass fraction of that component (except that hydrogen will capture twice as much energy per unit mass, because it has $Z/A = 1$). Then, if the total mass of the substrate (all mass except the Fe/Co/Ni clumps) is $M_{\rm sub}$, the gamma-ray energy deposited in a species s is

$$L_{{\rm dep},s} = \frac{k_{\rm dep} M_s}{M_{\rm sub} + M_{\rm H}} L_{\rm sub}\,, \quad (9)$$

where $k_{\rm dep} = 2$ for hydrogen and 1 for any other element. The fractions of $L_{{\rm dep},s}$ that go to ionization, nonthermal excitation, and heating, respectively, denoted by $\xi^{\rm io}$, $\xi^{\rm ex}$, and $\xi^{\rm ht}$, respectively, are given by Xu & McCray (1991) for hydrogen and by Kozma & Fransson (1992) for helium.

4. RADIATIVE PROCESSES AND LINE TRANSFER

4.1. *Optically Thick Line Transfer*

Here we consider the equations for ionization, recombination, and radiative transitions of hydrogen and helium in the case where recombination lines may be optically thick, following Xu et al. (1992). In the freely expanding envelope of a supernova, line transfer can be treated accurately with the Sobolev approximation (Sobolev 1957, 1960; Castor 1970; Mihalas 1978; Li & McCray 1993). In this approximation, the level population is calculated by replacing the normal spontaneous transition rate A_{ul} (Einstein A) by an effective transition rate $A^{\rm eff}_{ul}$, given by

$$A^{\rm eff}_{ul} = A_{ul} P_{\rm esc}(\tau_{lu})\,. \quad (10)$$

In our notation, the subscripts u and l represent the upper and lower levels, respectively, while i and j represent any levels. The escape probability of a line photon is given by

$$P_{\rm esc}(\tau_{lu}) = \frac{1 - \exp(-\tau_{lu})}{\tau_{lu}}\,, \quad (11)$$

and the Sobolev optical depth τ_{lu} by

$$\tau_{lu} = \frac{\pi e^2}{m_e c} f_{lu} \lambda_0 t N_l \left(1 - \frac{g_l N_u}{g_u N_l}\right) = \frac{\lambda_0^3 t}{8\pi} \frac{g_u}{g_l} A_{ul} N_l \left(1 - \frac{g_l N_u}{g_u N_l}\right), \quad (12)$$

where f_{lu} is the absorption oscillator strength, λ_0 is the line wavelength, g and N with subscripts are the statistical weights and population densities of the relevant level, t is the time since core collapse, and the term in parentheses accounts for induced emission.

If most of the atoms are in the ground state, such that $N_l \propto t^{-3}$, equation (12) implies that $\tau_{lu} \propto t^{-2}$ for resonance transitions.

If the emitting gas has uniform density and temperature, the observed flux is given by

$$F_{ul} = \frac{h\nu_{ul}}{4\pi D^2} N_u A_{ul}^{\rm eff} V f_z , \quad (13)$$

where $h\nu_{ul}$ is the energy of the line photon, D is the distance to the supernova, V is the volume of the emitting region, and f_z is the volume filling factor of the zone containing the emitting element. Equation (13) is valid for both the LTE and non-LTE cases, depending on the population N_u.

The above relations are valid provided that the continuum opacity to the line photons is negligible. But that is not the case for most UV lines in supernova envelopes. Therefore, to account for the loss of photons by continuum absorption processes such as ionization, dust absorption (discussed in more detail in § 6), or the pseudocontinuum absorption due to the many metal lines (Li & McCray 1996), we replace the escape probability $P_{\rm esc}$ in equation (10) by the total loss probability $P_{\rm loss}$ (Hummer & Rybicki 1985):

$$P_{\rm loss} = P_{\rm esc} + P_{\rm abs}(1 - P_{\rm esc}) , \quad (14)$$

where

$$P_{\rm abs} \approx \beta F(\beta) . \quad (15)$$

The parameter $\beta = \kappa_c/\kappa_l$ is the ratio of the continuum opacity,

$$\kappa_c = \sum_{s,j} N_{s,j} \sigma_{s,j} + \kappa_{\rm dust} + \kappa_{\rm metal} , \quad (16)$$

to the line core opacity,

$$\kappa_l = \frac{\tau_{lu}}{\Delta v_D \lambda_0 t} , \quad (17)$$

where $N_{s,j}$ is the number density of species s in state j, $\sigma_{s,j}$ is its ionization cross section, and $\Delta v_{\rm D}$ is the Doppler width of the line. For the continuum destruction probability of line photons, we use the expression given by Chugai (1987) for partial redistribution in an expanding atmosphere:

$$F(\beta) \approx 1.87 \left(\frac{a}{\beta}\right)^{1/4} , \quad (18)$$

where

$$a = \frac{A_{ul}}{4\pi \Delta v_{\rm D}} . \quad (19)$$

Equation (18) provides a good approximation for the strong resonance lines of interest here. The resulting absorption probability, which was also adopted by KF, is substantially less than the one derived for complete redistribution (Hummer 1968), which we used in our earlier work. Note that the flux escaping from the Sobolev sphere (eq. [13]) is calculated using the pure Sobolev $A_{ul}^{\rm eff}$, i.e., not the $A_{ul}^{\rm eff}$ including the continuum absorption terms.

Because we do not specify the geometrical distribution of the different composition zones in the envelope, there is some arbitrariness in accounting for sources of continuum opacity. We assume that most lines notice the average continuum opacity due to all of the zones, especially the dust in the iron zones, which forms at early times (see § 6). The only exceptions are the Lyα and He I λ584 lines, which we assume to be so highly trapped that they cannot diffuse out of the zone in which they are formed and therefore are sensitive only to the continuum opacity in the zone in which they are produced.

4.2. *Rate Equations*

The balance between ionization by nonthermal processes and radiative recombination determines the ionization state of the hydrogen and helium, and the radiative cascade following recombination determines the level populations and line strengths. In typical nebulae, the Lyman series is optically thick, while the Balmer and higher series of hydrogen lines remain optically thin. In this situation, called "case B" (Osterbrock 1989), the higher Lyman lines are resonantly trapped and converted into Lyα and Balmer and higher series photons.

As Xu et al. (1992) have described, in supernova envelopes the atomic densities can be so great that recombination lines in the Balmer and higher series can become optically thick as well. Accordingly, they defined "case C," in which the Balmer series is optically thick but the Paschen and higher series are optically thin; "case D," in which the Paschen series becomes optically thick; and so on. Since line optical depths decrease with time as $\tau \propto t^{-2}$, the recombination spectrum of SN 1987A evolved from case D to case C and, finally, to case B (Xu et al. 1992).

To study the evolution of the recombination spectrum in general, we solve the coupled rate equations describing the population of each level j:

$$N_j \left[\sum_i (N_e C_{ji} + A_{ji}^{\rm eff} + \zeta_{ji} + \chi_{ji}) + \Gamma_j\right] = \sum_i N_i (N_e C_{ij} + A_{ij}^{\rm eff} + \zeta_{ij} + \chi_{ij}) + N_e N^+ \alpha_j^{\rm eff} , \quad (20)$$

where N_e is the electron number density, C_{ji} is the collision coefficient, $\zeta_{ji} = B_{ji}^{\rm eff} J(\nu_{ji})$ is the stimulated transition rate due to the radiation field J at the line frequency ν_{ji}, χ_{ji} is the excitation rate directly by nonthermal electrons, N^+ is the number density of the singly ionized atoms, $\alpha_j^{\rm eff}$ is the "effective recombination coefficient" to level j, and Γ_j is the ionization rate from level j. The $B_{ji}^{\rm eff}$'s are related to the Einstein Bs by $B_{ji}^{\rm eff} = B_{ji} P_{\rm esc}(\tau_{ji})$ (Castor 1970). In equation (20) we have used the following notation: $A_{ji}^{\rm eff} = 0$ for $j \le i$, $B_{ji}^{\rm eff} = 0$ and $C_{ji} = 0$ for $j = i$.

We define the effective recombination coefficient by

$$\alpha_j^{\rm eff} = \left[P_{{\rm esc},j} + (1 - P_{{\rm esc},j}) \frac{\kappa_{c,j} - N_j \sigma_j}{\kappa_{c,j}}\right] \alpha_j , \quad (21)$$

where $\kappa_{c,j}$ is the continuum opacity for photons resulting from recombination to level j, and

$$P_{\rm esc,j} = \frac{3}{4\tau_j}\left[1 - \frac{1}{2\tau_j^2} + \left(\frac{1}{\tau_j} + \frac{1}{2\tau_j^2}\right)\exp\left(-2\tau_j\right)\right] \quad (22)$$

is the volume-averaged escape probability of the recombination continuum (Osterbrock 1989, Appendix 2), which has the limit $P_{\rm esc,j} \approx 1 - \tau_j$ for $\tau_j \ll 1$. The total continuum optical depth for the recombination photon is given by

$$\tau_j = \sum_z \kappa_{c,j,z} R f_z \ , \quad (23)$$

where $\kappa_{c,j,z}$ is the total continuum opacity at the threshold for ionization from level j (eq. [16]) in zone z, R is the radius of the envelope, and f_z the filling factor of zone z.

Note that, here and elsewhere, we approximate the emitting region from each element group as having uniform properties throughout. Since the continuum escape probability actually varies with position, the temperature and ionization must vary as well. By using volume-averaged escape probabilities, we suppress this variation.

The ionization rate from level j is given by

$$\Gamma_j = \Gamma_j^{\rm NT} + \Gamma_j^{\rm lines} + \Gamma_j^{\rm PH} \ , \quad (24)$$

where $\Gamma_j^{\rm NT}$ represents the contribution by nonthermal electrons. Assuming that the emitting region is illuminated uniformly by gamma rays, we can write this nonthermal ionization rate per atom of species s as

$$\Gamma_j^{\rm NT} = \frac{\xi^{\rm io} m_s}{\varepsilon_{\rm ph}[M_{\rm tot} + M_{\rm H}]} L_{\rm sub} \ , \quad (25)$$

where m_s is the atomic mass of species s, and $\varepsilon_{\rm ph}$ is its ionization potential.

We define

$$\Gamma_{s,j}^{\rm lines} = \sum_{s',u,l} \Gamma_{s,j,s',u,l}^{\rm line} \ , \quad (26)$$

where $\Gamma_{s,j,s',u,l}^{\rm line}$ is the photoionization rate from level j of species s due to absorption of a resonance line corresponding to a transition from level u to level l of species s',

$$\Gamma_{s,j,s',u,l}^{\rm line} = A_{ul,s'} P_{\rm abs} \frac{N_{s,j}\sigma_{s,j}}{\kappa_{c,s,j}} \frac{N_{s',u}}{N_{s,j}} \ . \quad (27)$$

In practice, we take only ionization by lines of H and He into account (s' = H, He).

We denote the continuum photoionization rate by

$$\Gamma_j^{\rm PH} = 4\pi \int_{\nu_j}^{\infty} \frac{J(\nu)}{h\nu} \sigma_j(\nu) d\nu \ , \quad (28)$$

where $\sigma_j(\nu)$ is the photoionization cross section of level j, and $J(\nu)$ is the mean intensity of the radiation field. We may write the mean intensity as the sum of contributions from different radiation mechanisms,

$$J(\nu) = J^{\rm H2q}(\nu) + J^{\rm He2q}(\nu) + J^{\rm Oth}(\nu) \ , \quad (29)$$

where the superscripts H2q, He2q, denote H I or He I two-photon continuum, and Oth denotes any other sources (such as UV lines from metals). Note that $J(\nu)$ includes neither the recombination-line photons, which are accounted for by $\Gamma_j^{\rm lines}$, nor the recombination continuum photons, which are accounted for by the $\alpha_j^{\rm eff}$ s.

We find that in our model the recombination timescales are always shorter than the timescale on which the ionization fraction is changing, so that the ionization state of hydrogen and primordial helium can be obtained from the steady state equations,

$$\sum_j N_j({\rm H})\Gamma_j({\rm H}) = N_e N_{\rm H^+} \alpha_t^{\rm eff}({\rm H}) \ , \quad (30)$$

and

$$\sum_j N_j({\rm He})\Gamma_j({\rm He}) = N_e N_{\rm He^+} \alpha_t^{\rm eff}({\rm He}) \ , \quad (31)$$

where the $\alpha_t^{\rm eff}$ s are the total effective recombination coefficients, given by

$$\alpha_t^{\rm eff} = \sum_j \alpha_j^{\rm eff} \ , \quad (32)$$

and N_e is the electron number density,

$$N_e = N_{\rm H^+} + N_{\rm He^+} \ . \quad (33)$$

The ionization of the helium zones has been discussed in detail by Li & McCray (1995). The main difference from the hydrogen zones is that photoionization of C I dominates the continuum opacity for the He I λ584 line. The electron density in the helium zones is determined by the ionization of helium, carbon, and oxygen,

$$N_e = N_{\rm He^+} + N_{\rm C^+} + N_{\rm O^+} \ , \quad (34)$$

so that we must consider in detail the ionization equilibrium of C and O. Just as in the hydrogen zone, we assume that the other metals are singly ionized.

4.3. *The Continuum Radiation Field*

4.3.1. H I *and* He I *Two-Photon Continua*

If the optical depth of Lyα, $\tau_{12} \gtrsim 10^9$, the H I 2P state of hydrogen becomes effectively metastable (Xu et al. 1992) and is depopulated by collisions with thermal electrons, which mix the 2S and 2P states. The H I 2S state and the He I 2 ^1S state decay by two-photon emission, with rates 8.22 and 51.3 s^{-1}, respectively. A fit to the results of Nussbaumer & Schmutz (1984) and Drake, Victor, & Dalgarno (1969) gives the following spectrum:

$$A(y) = A_0[1 - a(1-2y)^2 - b(1-2y)^4] \ , \quad (35)$$

where $y = \nu/\nu_{2q}$ is the ratio of the photon frequency ν to the frequency limit ν_{2q} of two-photon emission. For H I, $A_0 = 21.48$ s^{-1}, $a = 0.25$, and $b = 0.75$; for He I, $A_0 = 145$ s^{-1}, $a = 0.7$, and $b = 0.3$.

The volume-averaged escape probability of the two-photon continuum is given by $P_c(\tau_{2q})$ (eq. [22]), where $\tau_{2q} = \sum_z \kappa_{2q,z} R f_z$, and κ_{2q}, the continuum opacity of the envelope to the two-photon continuum, is given by equation (16).

The mean intensity of the two-photon continuum inside the envelope is given by

$$J^{2q}(\nu) \approx \frac{1 - P_c(\tau_{2q})}{\kappa_{2q}} \frac{1}{4\pi} N_u(2q) h\nu A(y) \ , \quad (36)$$

where h is Planck's constant, $N_u(2q)$ is the population density of the upper level that emits the continuum, and $P_c(\tau_{2q})$ has the same form as equation (22).

4.3.2. *The Pseudocontinuum Due to Metal Lines*

One of the major sources of uncertainty in our model is the effect of the opacity due to metal lines. It is dominated by many resonance transitions of iron group elements. Li &

McCray (1996) performed Monte Carlo simulations of the escape of two-photon continuum radiation through an expanding supernova envelope, and based on their results, we have modeled this metal opacity with a simple power-law approximation:

$$\kappa_{\rm metal} = 5 \times 10^{-23} N_{\rm H} \left(\frac{\lambda}{1216\ \text{Å}} \right)^{-5} . \quad (37)$$

Here, we have chosen to neglect the temperature dependence of this opacity, because it would just introduce another uncertain parameter into our model. We did calculate some models with a temperature-dependent metal-line opacity; but we found that such a temperature dependence does not strongly influence the results, because the effect of the metal opacity is largest at early times when the envelope has not yet cooled to very low temperatures. From equation (37) (and also directly from the detailed results of Li & McCray 1996) it follows that the metal opacity at Lyα is large, and we find that the probability that a Lyα photon is absorbed by metals after emission rather than scattered again is comparable to or larger than the probability for two-photon decay. A metal atom excited by a Lyα photon will decay and give rise to the emission of numerous metal lines that effectively form a continuum, as described by Li & McCray (1996). We do not attempt to model this process in detail here; instead, we approximate the resulting emission by a continuum with the shape of the hydrogen two-photon emission. We make the corresponding assumption for the He I λ584 line; but our results are insensitive to this assumption, since continuum absorption by neutral species (hydrogen, carbon) dominates the opacity at this wavelength.

We emphasize that this smooth metal-line spectrum is a crude approximation of the real UV spectrum, which will contain many features. Therefore, our predictions for the luminosity of some lines could be off by a significant factor, especially those that are pumped by UV photons. In § 8 we will discuss the influence of the metal opacity on our results, especially with respect to the hydrogen emission lines.

5. HEATING AND COOLING MECHANISMS

5.1. *Temperature Evolution*

To follow the temperature evolution, we solve the Second Law of Thermodynamics:

$$\frac{dE_{\rm th}}{dt} = L^{\rm heat} - C^{\rm cool} - \frac{2E_{\rm th}}{t} , \quad (38)$$

where $E_{\rm th} = 3[N_e + \sum_z N_z]kT/2$ is the thermal energy density, the term $2E_{\rm th}/t$ represents the adiabatic cooling resulting from the expansion of the envelope, and $L^{\rm heat}$ and $C^{\rm cool}$ are the net heating and cooling rates, respectively. Below we list the processes contributing to these rates.

5.2. *Heating Mechanisms*

5.2.1. *Nonthermal Electrons*

The dominant heating rate of the gas, due to Coulomb stopping of nonthermal electrons, is given by (see § 3)

$$L^{{\rm heat},\gamma} = \xi^{\rm ht} L_{\rm dep}(z) . \quad (39)$$

But the nonthermal electrons also deposit significant fractions of their energy as ionization and excitation, some of which also ultimately heat the gas. Therefore, to account accurately for the thermal evolution of the envelope, we must calculate the gas heating rate due to these processes as well, as we describe below.

5.2.2. *Photoionization*

The H I two-photon continuum can ionize hydrogen and helium atoms from levels 2 and higher, and the He I two-photon continuum can also ionize hydrogen from the ground state. This ionization provides extra heating for the gas. The net heating rate due to photoionization of atoms from level j is

$$L_j^{{\rm heat},2q} = N_u(2q) V f_z h\nu_{2q} \int_{x_j}^1 \xi_j(y) P_{\rm abs}^{2q}(y)(y - x_j) A(y) dy , \quad (40)$$

where V is the volume of the emitting region; f_z is the filling factor of the zone under consideration; $x_j = \varepsilon_{{\rm ph},j}/h\nu_{2q}$; and $P_{\rm abs}^{2q}$ is the absorption probability of two-photon emission by the envelope, given by

$$P_{\rm abs}^{2q} = 1.0 - P_c(\tau_{2q}); \quad (41)$$

ξ_j is the fraction of τ_{2q} that is due to the ionization of the atoms from level j; and $P_c(\tau_{2q})$ is given by equation (22).

Likewise, atoms can be ionized by resonance lines and thereby heat the gas. For example, the heating due to photoionization of hydrogen from the $n = 2$ level by Lyα is given by

$$L_2^{{\rm heat},{\rm Ly}\alpha} = N_2({\rm H}) A_{{\rm Ly}\alpha} \left[1 - \frac{\lambda_{{\rm Ly}\alpha}}{\lambda_{\rm thr}(n=2)} \right] h\nu_{{\rm Ly}\alpha} \times P_{\rm abs}({\rm Ly}\alpha) \frac{\kappa_c^i(n=2)}{\kappa_c({\rm Ly}\alpha)} , \quad (42)$$

where $\lambda_{\rm thr}(n = 2)$ is the wavelength of the Balmer continuum edge, $\kappa_c({\rm Ly}\alpha)$ is the total continuum opacity to Lyα, $\kappa_c^i(n = 2)$ is the Balmer continuum opacity to Lyα, and $P_{\rm abs}({\rm Ly}\alpha)$ is the total absorption probability of Lyα photons.

5.2.3. *Collisional De-excitation*

Collisional de-excitation from excited states of H and He that are either metastable or effectively metastable because of their high optical depth may contribute significant heating. This heating rate can be expressed as

$$L^{{\rm heat},{\rm coll}} = V f_z N_e \sum_{u,l} N_u C_{ul} h\nu_{ul} . \quad (43)$$

5.2.4. *Total Heating Rate*

Combining all of the above, the total heating rate is given by

$$L^{\rm heat} = \sum_{s={\rm H,He}} \times \left(L_s^{{\rm heat},\gamma} + \sum_j L_{j,s}^{{\rm heat},2q} + L_s^{{\rm heat},{\rm coll}} + L_s^{{\rm heat,lines}} \right) , \quad (44)$$

where $L_s^{\rm heat,lines}$ is the heating due to photoionization by lines, for example Lyα (eq. [42]).

5.3. *Cooling Mechanisms*

5.3.1. *Recombination*

Since the recombination cross section near threshold obeys the law $\sigma^{\rm rec} \propto v^{-2}$, the average thermal energy loss per recombination is kT. Therefore, the cooling rate due to

recombination of all species s is

$$C^{\rm recm} \approx Vf_z \sum_s kTN_e N_s x_s \sum_{j=1} \alpha_{j,s}^{\rm eff} , \quad (45)$$

where x_s is the ionization fraction.

5.3.2. *Bremsstrahlung*

The bremsstrahlung cooling rate due to all species s is (Osterbrock 1989)

$$C^{\rm brem} = 1.85 \times 10^{-27} \sum_s Z_s^2 T^{1/2} N_e x_s N_s Vf_z \text{ ergs s}^{-1} , \quad (46)$$

where x_s is the ionization fraction of species s, N_s its number density, and the mean Gaunt factor $g_{\rm ff}$ is chosen to be 1.3. Only bremsstrahlung by hydrogen and helium is taken into account.

5.3.3. *Thermal Impact Excitation*

Metals, e.g., Ca II and Fe II, are important thermal coolants in the envelope of SN 1987A. For example, the Fe II 26 μm line is excited by thermal electrons for all times considered here, and the [Ca II] λ7300 doublet is excited thermally for $t \lesssim 2$ yr. To calculate the thermal cooling rate by metals, we calculate non-LTE populations by equating radiative transition rates to thermal electron impact rates, excluding excitation and pumping by fast electrons, H I and He I two-photon continua, or any other UV lines. We denote $C^{\rm metal}$ as the total thermal cooling rate by metals.

We also include the cooling rates, $C^{\rm H}$ and $C^{\rm He}$, resulting from thermal electron impact excitation of H I and He I, respectively. Since the envelope is too cool for thermal excitation from the ground states of these atoms, these rates are dominated by excitation to higher levels from the effectively metastable H I $2S$ and He I $2\ ^3S$ states.

5.4. *Atomic Data and Processes*

We include all processes discussed above in our model: bremsstrahlung; radiative spontaneous transitions; thermal electron impact processes; excitation, ionization, and heating by nonthermal electrons; excitation and ionization by H I and He I two-photon continua; ionization of hydrogen and helium by H and He lines; Penning ionization; and recombination of hydrogen and helium. We also include the effects of dust grains: cooling by collisions, extinction of emission lines, and blocking of UV radiation.

Our model includes 20 states of H I, 31 singlet states and 30 triplet states of He I, 40 states of Ca II, 90 states of Fe II, 60 states of Co II, 40 states of Ni II, 42 states of C I, and 24 states of O I. For hydrogen, we assume complete l-mixing.

Energy levels and oscillator strengths are taken from Wiese, Smith, & Glennon (1966), Wiese, Smith, & Miles (1969), and Fuhr, Martin, & Wiese (1988). The collision strengths as functions of temperature for hydrogen transitions are taken from Aggarwal et al. (1991). The collision strengths for helium transitions are taken from Sawey & Berrington (1993). Photoionization cross sections of hydrogen and helium are obtained from TOPBase (Cunto & Mendoza 1993). The recombination coefficients for hydrogen are taken from Osterbrock (1989), if available, or calculated by using the Milne relation otherwise. The recombination coefficients for helium are the same as those used by Li & McCray (1995), and atomic data for Ca II and iron group elements are the same as those used by Li & McCray (1993) and Li et al. (1993).

6. DUST GRAINS

We shall see that dust grains, which evidently formed in the envelope of SN 1987A after $t \gtrsim 400$ days (see McCray 1993), play an important role in determining the emergent spectrum. Not only do the grains directly absorb radiation that would otherwise emerge, but they also affect it indirectly by absorbing the internal ultraviolet radiation field and to some extent by cooling the gas through gas-grain collisions.

6.1. *Dust formation in SN 1987A*

The first hint of thermal infrared emission from dust grains in the envelope of SN 1987A appeared as early as $t \sim 350$ days (Meikle et al. 1993). By $t \sim 450$ days, the appearance of a strong infrared continuum (Roche et al. 1989; Wooden et al. 1993; Meikle et al. 1993) simultaneous with the onset of substantial extinction of the optical continuum and the red sides of emission lines provided compelling evidence that a substantial amount of dust had formed in the envelope (Lucy et al. 1989).

Here we shall show that dust grains have two other effects. First, they reduce the UV pumping rates of metal lines, such as Ca II lines; second, they provide an additional mechanism for cooling the gas in the envelope of SN 1987A for $t \gtrsim 800$ days.

The different composition zones in the envelope have different temperatures, so the formation of dust will set in at a different time in each zone once the temperature has dropped below the sublimation point. The coolest zone is the Fe/Co/Ni zone modeled by Li et al. (1993), in which the temperature becomes low enough for dust formation between 300 and 400 days. This agrees well with the time the first signs of dust formation were observed. The hydrogen and helium zones modeled here are considerably hotter, and dust formation is unlikely to occur before ~ 800 days. We have used a simple fitting formula to describe the formation of dust as a function of temperature,

$$q_{\rm dust} = \begin{cases} q_0[1 - e^{-(T_c - T/\Delta T)^\gamma}] , & T < T_c , \\ 0 & T > T_c , \end{cases} \quad (47)$$

where $q_{\rm dust}$ is the fraction of the total amount of silicon that is bound in silicates for the hydrogen and helium zones and the fraction of the total mass that has condensed into dust for the iron zone. q_0, T_c, ΔT, and γ are fitting parameters that are adjusted to obtain an infrared luminosity light curve in agreement with the observed one.

We do not consider the dust formation process in detail, and in fact it is not completely clear that dust in the primordial zone will be able to form as quickly as required by the IR light curve, even though the temperature is low enough (D. Hollenbach 1997, private communication). Thus, some of the dust seen in the infrared may be formed in the other (O, Si) zones rather than in the H and He zones that we consider here. If this should be the case, it would not influence the extinction of most lines, since we assume anyway that line photons notice the continuum dust opacity averaged over all zones (see § 4.1). The one exception is Lyα, which could have a somewhat higher intensity in the internal radiation field if no dust is present in the H zone. This effect could play a role near the end of the time interval we

consider, when dust opacity due to dust in the H and He zones becomes comparable with the metal-line opacity in our models. However, in view of the theoretical uncertainties associated with dust formation and the fact that the continuum opacity at Lyα is already quite uncertain owing to the poorly known metal-line opacity, we think that our semiempirical approach is appropriate.

We assume that dust grains in the supernova envelope have a power-law size distribution:

$$n_d(a)da = k_d\, a^{-\alpha}\, da\ , \tag{48}$$

where a is the radius of the grain. For interstellar grains, the index $\alpha = \alpha_1 = 3.5$ for $a \lesssim a_1 = 0.2$ μm and $\alpha = \alpha_2 > 4$ for $a > 0.2$ μm (Draine 1995). For the envelope of SN 1987A we assume $\alpha_1 = 3.5$ and $\alpha_2 = 4.5$. Moreover, we assume that this distribution extends to grains as small as $a_{\rm min} = 10^{-3}$ μm. The small grains will dominate the gas cooling and ultraviolet extinction, while the larger grains, which comprise most of the net mass in grains, will dominate the infrared extinction.

6.2. *Extinction*

The opacity due to dust grains is given by

$$\kappa_{\rm dust} = \int Q(a,\, \lambda)\sigma_d\, n_d(a)da\ , \tag{49}$$

where $\sigma_d = \pi a^2$; $Q(a, \lambda)$ is the absorption coefficient of the grain, which can be written as

$$Q(a,\, \lambda) \approx \begin{cases} 1\ , & \lambda < \epsilon a\ , \\ \epsilon a/\lambda\ , & \lambda \geq \epsilon a\ ; \end{cases} \tag{50}$$

and ϵ is a factor depending on wavelength. For silicate grains, Draine & Lee (1984) suggest

$$\epsilon \approx \begin{cases} 1 & \lambda < 0.2\ \mu\text{m}\ , \\ \frac{1}{3} & \lambda \geq 0.2\ \mu\text{m}\ . \end{cases} \tag{51}$$

For wavelengths in the range $0.06\ \mu\text{m} \lesssim \lambda \lesssim 1\ \mu$m we find from equations (49), (50), and (51),

$$\kappa_{\rm dust} \approx \frac{3}{4\pi R^3}\,\frac{\epsilon}{\lambda}\,\frac{3}{4\rho_d}\,M_d, \tag{52}$$

where M_d is the total mass of dust grains, given by

$$M_d = \int_{a_{\rm min}}^{a_{\rm max}} \frac{4\pi}{3}\, a^3 \rho_d\, n_d(a)da\ , \tag{53}$$

and $\rho_d \sim 3$ g cm^{-3} is the density of the grain material.

By using equation (52), we implicitly assume that the dust is rather finely distributed throughout the envelope, and that the internal extinction can be described with a $1/\lambda$ law. If the dust is concentrated in a number of dense clumps that have very large optical depth but do not cover the envelope completely, as has been suggested by Lucy et al. (1989), we are probably overestimating the effects of extinction, especially for shorter wavelengths.

6.3. *The Influence of Dust on the Thermal Balance*

When an atom, a thermal electron, or an ion collides with a dust grain, it will lose all or part of its thermal energy.

We calculate the cooling due to collisions of grains and charged particles according to the prescription of Draine & Sutin (1987). The total cooling rate due to collisions between thermal electrons and silicate grains with the size distribution given by equation (48) is

$$C^{d,e} = \frac{1}{2}\, N_e kT\left(\frac{8kT}{\pi m_e}\right)^{1/2} p_e\,\frac{3}{4\rho_d}\,\frac{M_d}{(a_{\rm max}^{0.5} - a_{\rm min}^{0.5})} \times \int \tilde{\Lambda}(Z_d,\, T)a^{-1.5}\, da\ , \tag{54}$$

in which $p_e(\sim 1)$ is the sticking coefficient for electron-grain collisions, Z_d is the grain charge, and the function $\tilde{\Lambda}$ is given in Draine & Sutin (1987). Cooling due to collisions of ions with grains is negligible.

Since the ionized fraction in the envelope of SN 1987A is low, collisions of neutral atoms with grains are far more frequent than collisions of ions with grains, and so they will dominate the gas-grain cooling. For a size distribution given by equation (48), Burke & Hollenbach (1983) derive a total cooling rate due to the collision between dust gains and hydrogen atoms of

$$C^{d,\rm H} = 2N_{\rm H} kT\left(\frac{8kT}{\pi m_{\rm H}}\right)^{1/2} \bar{\eta}_{\rm H}\,\frac{3}{4\rho_d}\,M_d\left(1 - \frac{T_d}{T}\right)\frac{1}{(a_{\rm min}\, a_{\rm max})^{0.5}}\ , \tag{55}$$

where T_d is the temperature of the dust grains, and $\bar{\eta}_{\rm H}$ is the average accommodation coefficient of hydrogen on the grain surface. For silicate grains, $\bar{\eta}_{\rm H} \sim 0.2$ in the temperature range of our study (Burke & Hollenbach 1983). The dust temperature T_d is taken from Wooden et al. (1993), although its effect in equation (55) is negligible. The cooling rate due to collisions between helium atoms and dust grains, $C^{d,\rm He}$, can be estimated approximately by using equation (55) and replacing $N_{\rm H}$, $m_{\rm H}$, and $\bar{\eta}_{\rm H}$ with $N_{\rm He}$, $m_{\rm He}$, and $\bar{\eta}_{\rm He}$, respectively. We assume $\bar{\eta}_{\rm He} = 0.2$ in our work. The substantial uncertainty in $\bar{\eta}_{\rm He}$ does not cause a big error in our results, because in the hydrogen zone $C^{d,\rm He}$ is always much smaller than $C^{d,\rm H}$ and $C^{d,e}$ (eq. [54]), and even in the helium zones, $C^{d,\rm He}$ is still smaller than $C^{d,e}$.

Combining these three cooling rates by dust grains yields the total dust cooling rate

$$C^{\rm dust} = C^{d,\rm H} + C^{d,\rm He} + C^{d,e}\ . \tag{56}$$

The collisional processes discussed above give an upper limit on the cooling rate by dust, since the dust may also contribute to the heating, especially through the grain photoelectric effect. We did not include this process in our model, since it is quite complex to model and depends strongly on poorly known parameters such as dust size distribution, composition, and environmental conditions (e.g., Bakes & Tielens 1994), and thus it would introduce even more free parameters. Furthermore, for the UV photons that contribute most to the photoelectric heating, we find that the continuum opacity due to hydrogen and the pseudocontinuum opacity due to metal lines is significantly higher than the dust opacity over most of the evolution, so that the grain photoelectric effect is unlikely to be energetically important.

7. NUMERICAL METHOD

We use the following procedure to determine the temperature and ionization and to calculate emission-line luminosities. As mentioned above, the timescales for the gas to reach equilibrium in the level populations is very short

compared to the age of the supernova. As we shall see in § 8.1.2, the ionization timescale is also always at least 5 times shorter than the age. The thermal timescale, however, becomes comparable to the age of the supernova around 500 days, so that we must solve the time-dependent equation (38). We start by assuming a temperature at $t = 200$ days, and we solve the coupled equations (20), (30), and (31) to determine the non-LTE level populations and the ionization balance. Then, given N_e (eq. [33]), we calculate the fractions $\xi^{\rm io}$, $\xi^{\rm ex}$, and $\xi^{\rm ht}$ of gamma-ray energy that are deposited as ionization, excitation, and heat, and we iterate between these two steps until a consistent set of ionization states, level populations, and nonthermal ionization and excitation rates is obtained.

Then we evaluate the other heating and cooling rates discussed in § 5, and we solve equation (38) for the temperature at the next time step. Since the heating and cooling timescales are initially very short compared to the age of the supernova, we must use an implicit method to solve the differential equation for the temperature. We use a differencing scheme of the form

$$T_{n+1} = T_n + \left[\epsilon\left(\frac{dT}{dt}\right)_n + (1-\epsilon)\left(\frac{dT}{dt}\right)_{n+1}\right](t_{n+1} - t_n)\,. \tag{57}$$

Since $(dT/dt)_{n+1}$ depends very nonlinearly on T_{n+1}, we must iterate to solve this equation, starting with an initial guess at T_{n+1} and improving it using the secant method until equation (57) is fulfilled. Convergence to within 0.01 K is generally reached after three or four iterations. For the first few steps in which the temperature rapidly approaches equilibrium, we take $\epsilon = 0$ for the highest stability, and later we change to $\epsilon = 0.5$ for better accuracy.

Finally, given the values of temperature, ionization, and non-LTE level populations, we calculate the emergent luminosities of all emission lines of hydrogen, helium, and trace metals.

8. RESULTS

8.1. *Physical Conditions*

8.1.1. *Temperature and Density*

Figures 1*a* and 1*b* show the evolution of the temperature and the density in the three different composition zones. Although the density is simply determined by the homologous expansion and our choice of masses and filling factors, we show it here because it is important for understanding what physical processes are important and for comparison with other work. The temperature in the hydrogen zone decreases from $T = 6000$ K at $t = 200$ days to $T = 1200$ K at $t = 1200$ days. The temperatures in the helium zones are somewhat less than that of the hydrogen, especially in the carbon-rich helium zone, which evolves from 5100 to 700 K at 1200 days.

We find that these results are rather insensitive to the assumptions of the model. Alternative choices for the metal opacity or the abundances can cause a maximum variation of about 400 K at 300 days for the H and He (carbon-poor) zone 2. The carbon-rich He zone shows a stronger dependency, increasing by as much as 700 K at 200 days if the carbon abundance is reduced by a factor of 3.

Figure 2 shows the fractional contributions of the different physical processes to the heating and cooling rates in the hydrogen zone. The heating is generally dominated by nonthermal electrons depositing their energy directly into the free electron gas (*solid curve*), except for early times when heating due to photoionization of H from $n = 2$ by the hydrogen two-photon continuum contributes significantly. The curve labeled "collisions" represents the net heating rate due to collisional transitions in H and He. When the net effect of collisions is heating, it appears as a heating term, and when it is cooling it appears as a cooling term. Collisional de-excitation (heating) always dominates at later times. The main transition responsible for this heating is the forbidden transition from the lowest He I triplet state ($2\,^3S$) to the ground state ($1\,^1S$). The $2\,^3S$ state is efficiently populated by nonthermal excitation or recombination into any triplet state followed by radiative decay. The line labeled "He584" represents the heating due to photoionization of hydrogen by the He I λ584 line. Note that at early times the total heating rate is essentially independent of the detailed physical mechanisms, since most of the direct products of the nonthermal energy deposited in excitation and ionization (recombination continuum, lines, two-photon continuum) cannot escape from the highly opaque envelope, and their energy ends up in the thermal pool by some process or another. This situation starts to

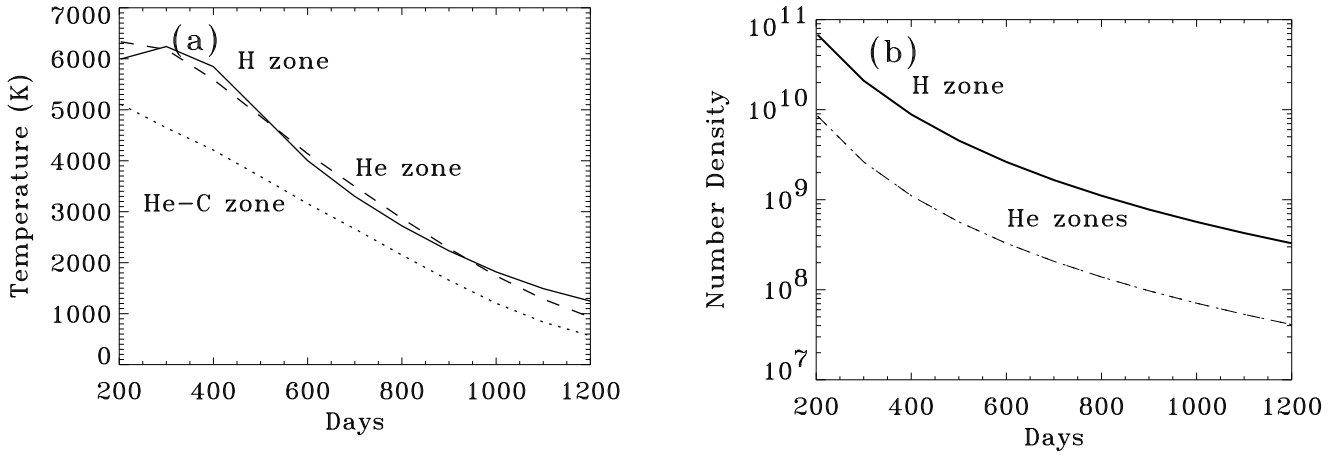


FIG. 1.—Evolution of (*a*) temperature and (*b*) density in the three composition zones. (*a*) *Solid line:* Hydrogen zone; *dotted line:* carbon-rich helium zone; *dashed line:* carbon-poor helium zone. (*b*) *Solid line:* Hydrogen zone; *dash-dotted line*: helium zones.

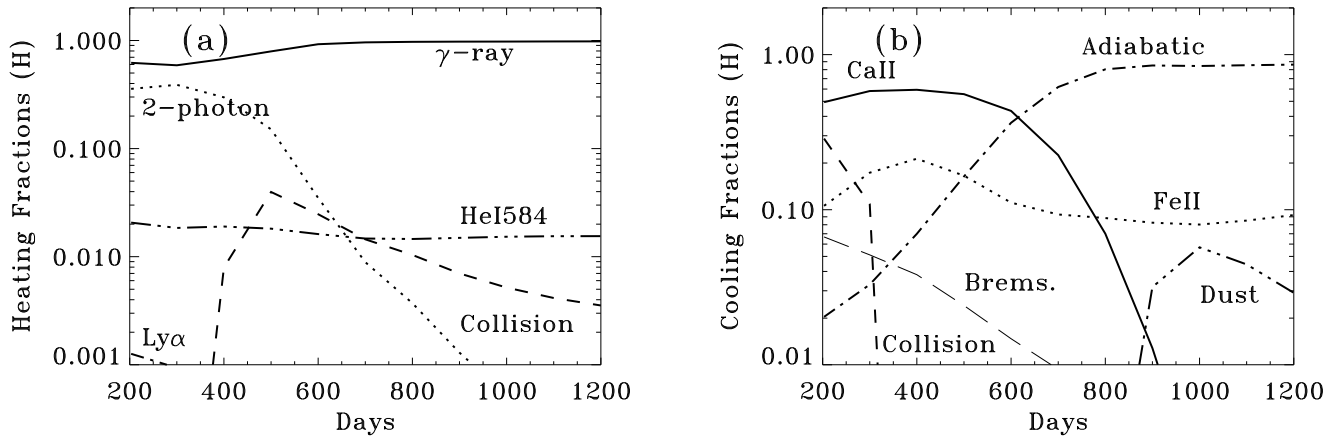


FIG. 2.—(*a*) Heating rate and (*b*) cooling rate fractions in the hydrogen zone. Curves refer to the following processes: (*a*) *Solid*, gamma-ray heating; *dashed*, collisional processes of H and He; *dot- dashed*, ionization by Lyα; *dotted*, ionization by H I and He I two-photon continua; *three-dot–dashed*, ionization by the He I λ584 line. (*b*) *Solid*, total Ca II line emission; *dotted*, total Fe II line emission; *dot-dashed*, adiabatic; *dashed*, collisional processes; *three-dot–dashed*, dust; *long-dashed*, thermal bremsstrahlung.

break down when dust absorption becomes important and when substantial radiation can escape directly.

For $t \lesssim 600$ days, the hydrogen zone cools primarily by the emission of thermally excited emission lines, mainly (~60%) [Ca II] λ7300 (Li & McCray 1993), but also including significant contributions from [Fe II] 26.0 μm (10%–20%). At 200 days the net effect of collisional processes in H and He is still cooling (~30%), but this term drops rapidly, changing to net heating at 400 days. Bremsstrahlung contributes a few percent to the cooling at early times. For $t \gtrsim 600$ days, adiabatic losses dominate the cooling, and at about the same time thermal equilibrium can no longer be maintained, and time-dependent cooling sets in. Cooling by collisions of atoms with dust grains reaches a maximum of 5% of the total cooling rate around 1000 days.

Figure 3 shows the fractional contributions to heating and cooling rates of the two helium zones. Direct heating by nonthermal electrons is more dominant in the carbon-rich He zone 1, because ionized carbon contributes substantially to the free-electron density. The heating due to photoionization of C I by He I λ584 is also stronger in the carbon-rich zone 1. In both He zones, but especially in the carbon-poor zone 2, heating by collisional de-excitation of the metastable 2^3S level of He I contributes substantially at later times.

In He zone 1, the radiative cooling for $t \lesssim 700$ days is dominated by several infrared emission lines of C I, resulting in a somewhat lower temperature, while in zone 2 it is dominated by [Ca II] λ7300 and [Fe II] 26.0 μm. In both helium zones, radiative cooling (mainly due to [Fe II] 26.0 μm) remains comparable to adiabatic cooling even for $t \gtrsim 700$ days.

Since radiative cooling in the hydrogen zone is negligible after 1200 days (Fig. 2), the temperature will decrease thereafter as $T \propto t^{-2}$. This result implies a temperature $T(2210 \text{ days}) = 350$ K, a value consistent with the value $T(2210 \text{ days}) = 400 \pm 100$ K inferred by Wang et al. (1997) from *HST* observations of the width of the Balmer continuum emission feature at that time.

8.1.2. *Ionization*

Figure 4*a* shows the evolution of the ionization fractions $x_H = H^+/H$ and $x_{He} = He^+/He$ in the hydrogen and helium zones.

The hydrogen ionization fraction evolves from $x_H \approx 7 \times 10^{-3}$ at $t = 200$ days to $x_H \approx 3 \times 10^{-4}$ at $t = 1200$ days. [This fraction is slightly lower than that found by Xu et al. (1992), who did not calculate temperature evolution but simply assumed $T = 3000$ K for all times.] At late times, $x_{He} > x_H$ owing to a somewhat lower recombination rate coefficient and somewhat higher ionization rate by nonthermal electrons. But at early times, photoionization of hydrogen from excited states causes $x_H > x_{He}$. In the helium zones, the ionization level x_{He} is greater than that in the hydrogen zone, because the electron number densities in the helium zones are less than half that in the hydrogen zone. Our values for the ionization level at 300 days are about one-half those found by KF. The difference can be attributed to the lower gas density in their model.

Figure 4*b* shows the evolution of the main ionization mechanisms of hydrogen as fractions of the total ionization rate. One sees that the ionization after 450 days is dominated by stopping of nonthermal electrons (*solid curve*), while for $t \lesssim 450$ days, Balmer continuum photoionization by the hydrogen two-photon continuum is more important. Xu et al. (1992) pointed out that such photoionization from excited states is required to account for the luminosities of hydrogen recombination lines at early times. Excited helium atoms also contribute a few percent to the ionization of hydrogen through the Penning process and through photoionization by He I λ584.

Kozma & Fransson (1993) pointed out that the bolometric luminosity of SN 1987A may exceed the instantaneous radioactive-energy deposition rate if the recombination timescale in the envelope becomes longer than the supernova age. In their model, delayed recombination, or "ionization freezeout," became an important source of luminosity in the outer envelope for $t \gtrsim 800$ days. In our model, however, instantaneous ionization balance still

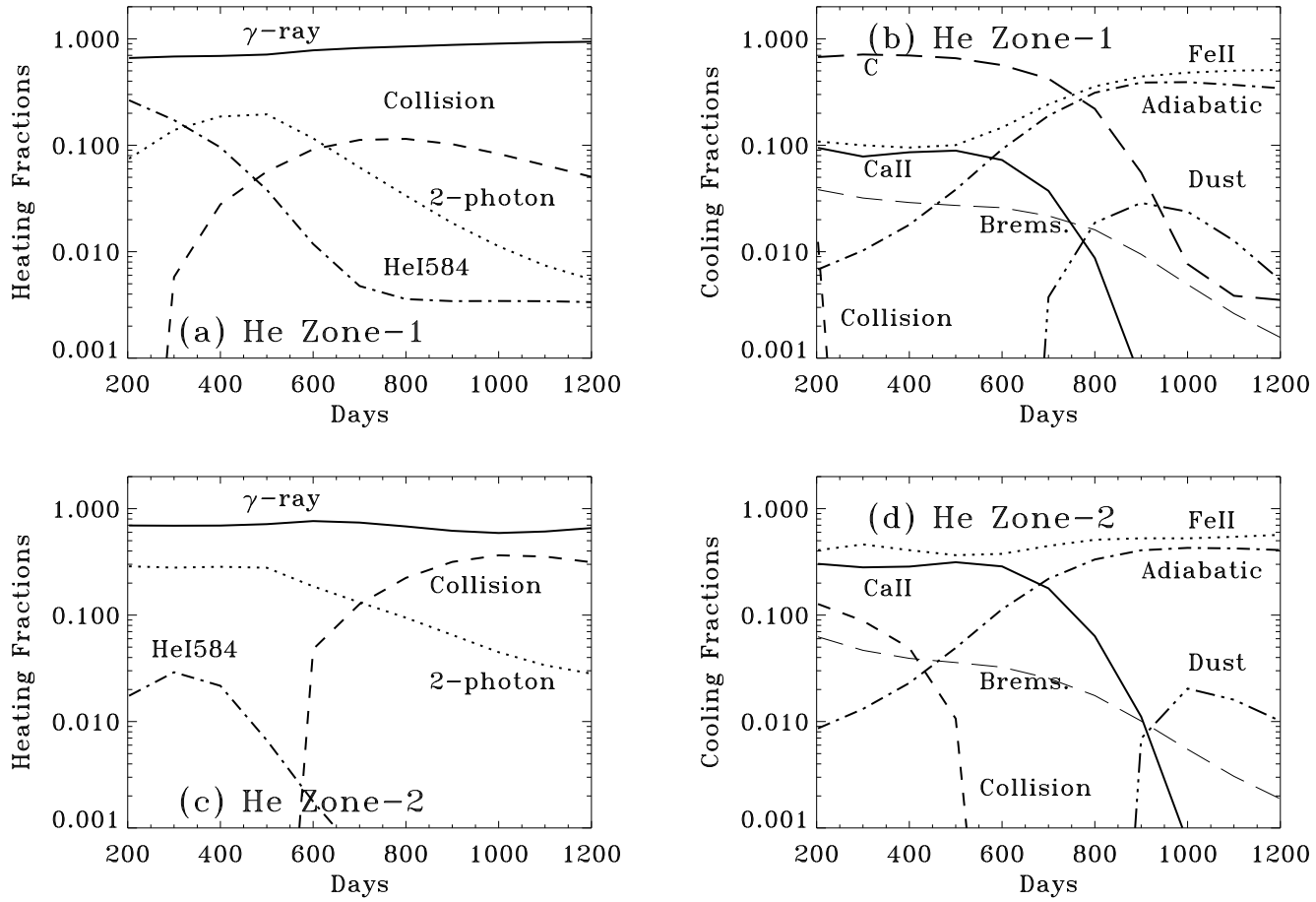


FIG. 3.—(*a*, *c*) Heating rate and (*b*, *d*) cooling rate fractions in the helium clumps: (*a*, *b*) Carbon-rich; (*c*, *d*) carbon-poor. (*a*, *c*) *Solid curve:* Gamma rays; *dashed curve:* collisional processes of He; *dotted curve:* ionization by He I two-photon continuum; *dot-dashed curve:* ionization by the He I λ584 line. (*b*, *d*) *Solid curve:* Total Ca II line emission; *dashed curve:* collisional; *dotted curve:* total Fe II line emission; *dot-dashed curve:* adiabatic; *thick long-dashed curve:* total C I line emission; *thin long-dashed curve:* thermal bremsstrahlung; *three-dot–dashed curve:* dust.

applies at 1200 days, at which time the recombination time is still ~5 times shorter than the timescale on which the ionization fraction is changing. Our result differs from that found by Kozma & Fransson because we assume a higher density of hydrogen in the inner envelope than they did, and we do not consider emission from the lower density outer envelope.

Nevertheless, the bolometric luminosity in our model can still exceed the energy deposition rate, because the radiative cooling timescale exceeds the age of the envelope. With KF,

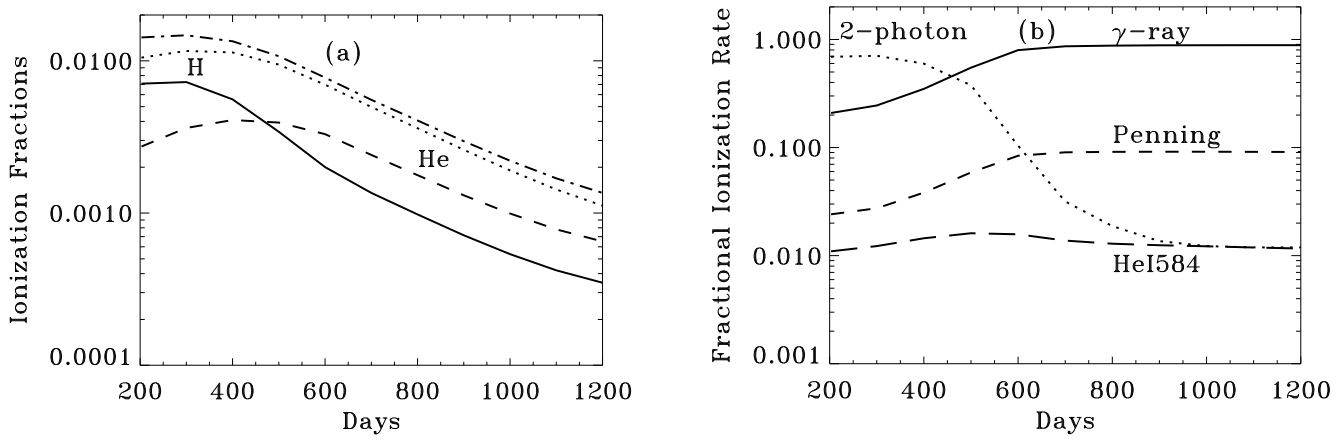


FIG. 4.—Evolution of the ionization fractions in the three composition zones (*a*) and the fractional ionization rates of hydrogen (*b*). (*a*) *Solid line:* H in H zone; *dashed line:* He in H zone; *dash-dotted line:* He in carbon-rich helium zone; *dotted line:* He in carbon-poor He zone. (*b*) *Solid line:* γ-rays; *dashed line:* Penning; *long-dashed line:* ionization by the He I λ584 line; *dotted line:* H I and He I two-photon continua; *dot-dashed line:* Lyα; *three-dot–dashed line:* Hα.

we find that this "thermal freezeout" occurs earlier than ionization freezeout.

8.2. *Emission Lines*

8.2.1. Ca II

Li & McCray (1993) showed that the light curves of infrared emission lines of Ca II are sensitive to the temperature evolution of the hydrogen. As we have seen above, this temperature is mainly determined by a balance between radioactive heating and cooling by thermal impact excitation of Ca II lines for $t \lesssim 600$ days and by adiabatic expansion thereafter.

Since gas with $T \lesssim 5000$ K is too cool to excite the Ca II $4p^2P$ level, the Ca II λ8600 infrared triplet can only be excited by ultraviolet pumping in the Ca II H and K lines for $t \gtrsim 400$ days. Li & McCray (1993) characterized this pumping rate by a free parameter. Here, we actually calculate it from the ultraviolet continuum at 3900 Å, which is produced by H I and He I two-photon decays and by the decay of metal atoms excited by Lyα (§ 4.3).

Figures 5*a* and 5*b* compare the light curves of two calcium lines, [Ca II] λ7300 and Ca II λ8542, with observations. The light curve for the Ca II λ8662 line is virtually identical to that of the Ca II λ8542 line. The thick solid curve is the total emission of Ca II, including primordial gases (*dashed curve*), helium zone 1 (*dotted curve*) and zone 2 (*dot-dashed curve*), respectively. The thick dashed curve is the total emission before the extinction correction is applied.

The 3900 Å continuum around the H and K lines is mainly absorbed by metal opacity and dust grains, which makes the strengths of the Ca II λ8600 lines somewhat dependent on our choice for the metal opacity. As expected, a lower metal opacity leads to a stronger continuum and a stronger Ca II λ8600 infrared triplet. For our standard assumptions, the dominant continuum opacity at 3900 Å for $t \lesssim 550$ days is metal lines, after which dust becomes more important. We consider the uncertainty in UV continuum to be the most likely cause of the small discrepancy between our model and the observed Ca II λ8600 lines, which occurs mainly between 400 and 600 days.

For $t \gtrsim 1000$ days, the predicted flux of [Ca II] λ7300 in Figure 5*a* is substantially lower than observed. The same discrepancy was found by KF. They argue that observations of the 3900 Å continuum at 1046 days show that it is stronger than expected for the simple two-photon estimate, and that the energy that can be absorbed in the H and K lines roughly corresponds to the observed total flux in the [Ca II] λ7300, Ca II λ8542, and Ca II λ8662 lines.

8.2.2. *Iron*

Li et al. (1993) calculated models for the thermal evolution and line emission of the newly synthesized Fe/Co/Ni in the envelope of SN 1987A. They showed that the newly synthesized iron group elements must occupy roughly half the volume of the emitting region, and they argued that this relatively large filling factor is the natural result of the expansion of Ni bubbles as a result of radioactive heating that took place in the newly synthesized ^{56}Ni during the first few weeks after explosion. Li et al showed that emission from the iron group bubbles could account quantitatively for the light curves of the infrared emission lines of Fe/Co/Ni for $t \lesssim 600$ days. The model failed to account for the brightness of most such lines for $t \gtrsim 600$ days, however.

Here we find that the emission lines of Fe/Co/Ni at $t \gtrsim 600$ days are produced, not by newly synthesized Fe/Co/Ni, but by primordial iron group elements in the hydrogen and He zones. Figures 6*a*–6*c* show the light curves of three such lines, [Fe II] 1.26 μm, [Fe II] 26.0 μm, and [Fe II] 7157 Å, respectively.

Consider first the [Fe II] 1.26 μm line (Fig. 6*a*). According to Li et al. (1993), the emission by Fe/Co/Ni clumps could account well for this feature until day $\sim$600, but it failed after then. Their result is replotted here (*thin three-dot–dashed curve*). Here we find that for $t \gtrsim 600$ days primordial iron in the H and He zones contributes a substantial fraction to this emission feature. By adding the emission by Fe/Co/Ni clumps and the emission by the primordial iron together (*thick three-dot–dashed curve*), the predicted light curve of [Fe II] 1.26 μm is close to the observed one. The remaining discrepancy probably comes from the surface of Fe/Co/Ni clumps. We believe that UV pumping in the surface layer of Fe/Co/Ni clumps, which was not included

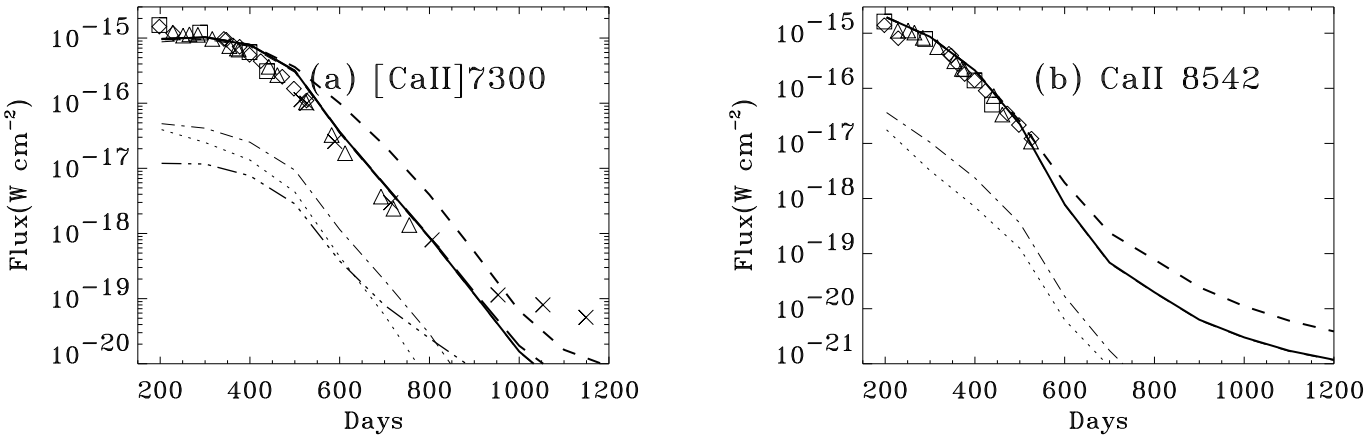


FIG. 5.—Light curves of Ca II emission lines: (*a*) [Ca II] λ7300 (including [Ni II] λ7378); (*b*) Ca II λ8542. *Solid curve:* Total emission, including effects of dust; *thick dashed curve:* without extinction; *thin dashed curve:* hydrogen zone; *dotted curve:* helium zone 1; *dot-dashed curve:* helium zone 2. (*a*) *Three-dot–dashed curve:* [Ni II] λ7378. Observations: *diamonds*, Phillips et al. (1990); *triangles*, Spyromilio et al. (1991); *squares*, Terndrup et al. (1988); *crosses*, Suntzeff et al. (1991).

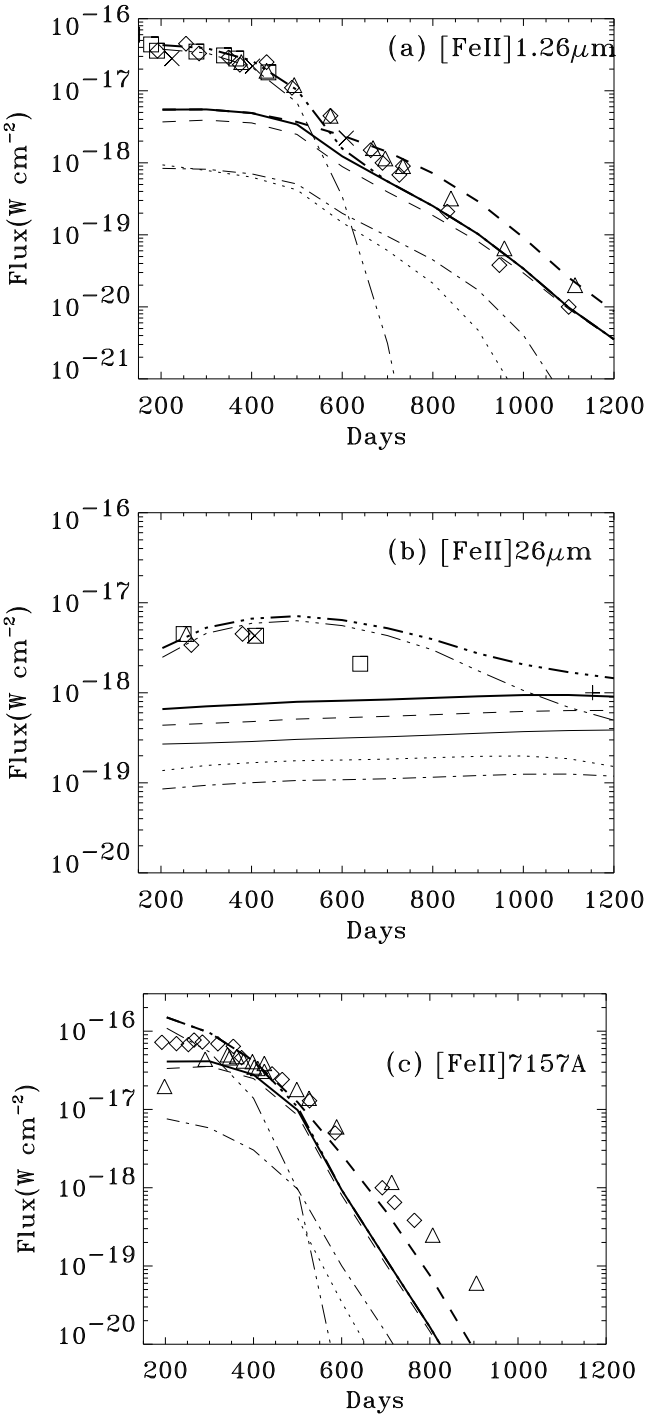


FIG. 6.—Light curves of Fe II lines: (*a*) [Fe II] 1.26 μm, (*b*) [Fe II] 26.0 μm, and (*c*) [Fe II] λ7157. *Thick solid line:* Total emission from H and He zones; *thick three-dot–dashed line:* sum of the emission by Fe/Co/Ni clumps and the emission by the H and He zones; *dashed line:* hydrogen zone; *thin three-dot–dashed line:* emission by Fe/Co/Ni clumps (from Li et al. 1993); *dotted line:* helium zone 1; *dot-dashed line:* helium zone 2. Observations of [Fe II] 1.26 μm: *diamonds:* Meikle et al. (1989); *triangles:* Meikle et al. (1993); *squares:* McGregor (1988); *crosses:* E. Oliva (1994, private communication). Observations of [Fe II] 26.0 μm: *diamonds:* Moseley et al. (1989); *triangles:* Erickson et al. (1988); *squares:* Colgan et al. (1993); *crosses:* Haas et al. (1990); *plus signs:* Dwek et al. (1992). Observations of [Fe II] λ7157: *diamonds:* Spyromilio et al. (1991); *triangles:* Phillips & Williams (1991).

by Li et al. (1993), will be important for this emission feature.

We see that [Fe II] 26.0 μm (Fig. 6*b*) is emitted mainly by Fe/Co/Ni clumps for $t \lesssim 1000$ days, but that primordial iron contributes a substantial fraction to this feature at later times. The flux from the iron in the primordial zone is nearly constant, because the emitting regions are optically thin, in LTE, and they have a temperature much greater than the energy difference between the levels, so that the luminosity depends only on the Fe II mass. At much later times (~ 10 yr), the temperature in the primordial zones will become too low to excite the upper level, while the extra energy released in the Fe/Co/Ni clumps by positrons resulting from Ti^{44} decay will cause the iron clumps to be hot enough to be the main source of the [Fe II] 26.0 μm luminosity again.

The present model predicts a flux of [Fe II] λ7157 (Fig. 6*c*) that is considerably less than observed for $t \gtrsim 500$ days, as also found by Li et al. (1993), who considered only emission from the iron clumps. Although the emission from the primordial zone is now included, and it indeed dominates at later times, the total flux is still not sufficient to match the observations. Just as in the case of Ca II, we suspect that our inadequate treatment of the UV flux is the main cause of the discrepancy. Support for this explanation is found in the work of Li & McCray (1996), who consider the UV field inside the remnant in greater detail. They find that [Fe II] λ7157 is one of the stronger emission lines in the emerging spectrum at 800 days. Other simplifications in the present work that could lead to an underestimate of the [Fe II] λ7157 line are the neglect of nonthermal ionization and excitation and photoionization of Fe II. However, simple energy arguments suggest that possible corrections for these processes are insufficient to explain the large observed flux. We note that KF were able to reproduce the [Fe II] λ7157 line satisfactorily. We do not know why our result differs from theirs.

8.2.3. *Hydrogen*

Given an acceptable fit to Ca II and Fe II lines, the fit of our model to the light curves of other emission lines, especially the hydrogen lines, becomes an important check on our physics. The results are shown in Figures 7 and 8, together with the observed data. Again, thick solid curves in these figures are the emission including dust extinction. Figure 7 shows Hα, Hβ, Paα, and Paβ. Figure 8 shows four Brackett lines.

To illustrate when the transitions between the different regimes of hydrogen line formation occur, we have plotted in Figure 9*a* the optical depths of Hα, Hβ, Hγ, and the Balmer continuum, and in Figure 9*b* those of Paα, Paβ, Paγ, and the Paschen continuum. The Paschen continuum is optically thick for $t \lesssim 150$ days, and the Balmer continuum is optically thick for $t \lesssim 500$ days. The recombination spectrum (Xu et al. 1992) corresponds to case D (Paβ optically thick) for $t \lesssim 400$ days, to case C (Hβ optically thick) for $400 \lesssim t \lesssim 800$ days, and to case B thereafter.

Figures 7*a*–7*d* show the light curves of Hα, Hβ, Paα, and Paβ, respectively. One sees that the theoretical curves (*solid curves*) roughly follow the observed data, but some significant discrepancies remain. We find that two of our assumptions are especially important for the hydrogen lines: the metal opacity at the wavelength of Lyα and the continuum absorption probability in equation (18). Both assumptions

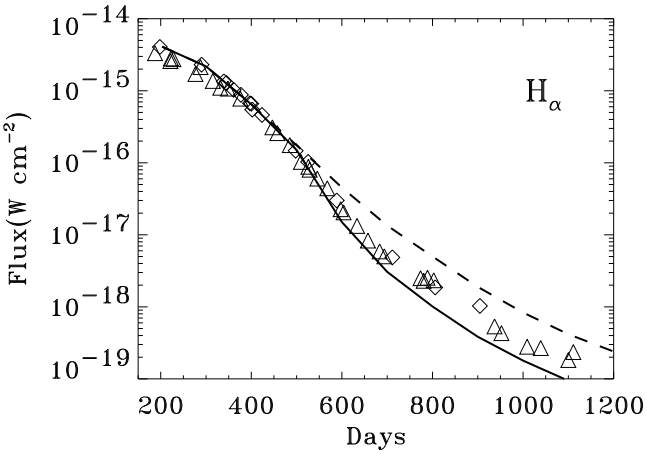


FIG. 7*a*

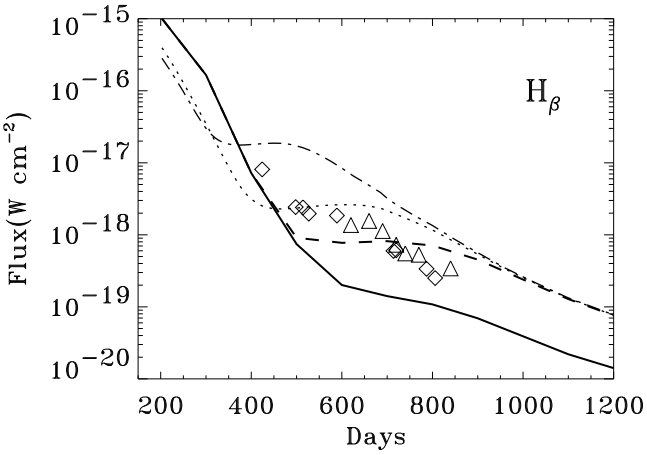


FIG. 7*b*

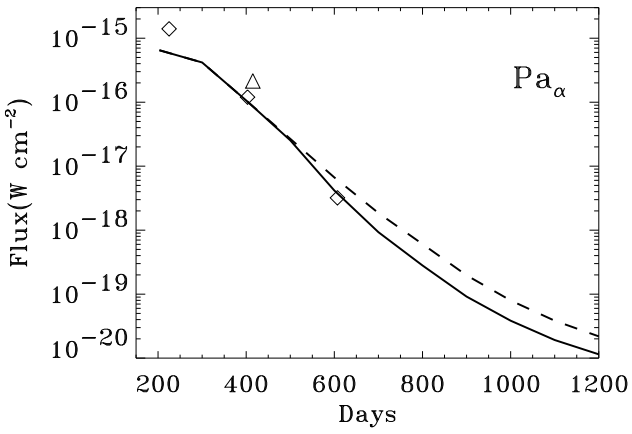


FIG. 7*c*

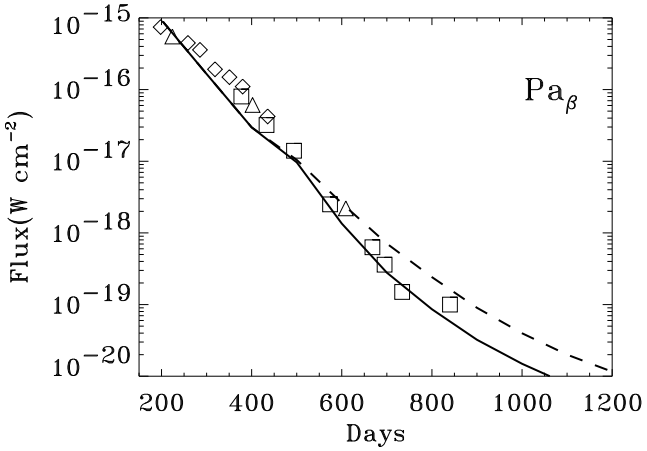


FIG. 7*d*

FIG. 7.—Light curves of Balmer and Paschen series. *Solid line:* Observable flux; *thick dashed line:* without extinction. (*b*) *Dotted line:* Metal-line opacity increased by a factor of 10; *dot-dashed line:* line photon continuum destruction probabilty for complete redistribution. Observations of Hα: *diamonds*, Phillips & Williams (1991); *triangles*, Danziger et al. (1991). Observations of Hβ: *diamonds*, Phillips et al. (1990); *triangles*, J. W. Menzies (1990, private communication). Observations of Paα: *diamonds*, E. Oliva (1994, private communication); *triangles*, Wooden et al. (1993). Observations of Paβ: *diamonds*, Phillips & Williams (1991); *triangles*, E. Oliva (1994, private communication); *squares*, Meikle et al. (1993).

affect the $n = 2$ level population of hydrogen, since they determine the density of Lyα photons that support this population. They also affect the populations of the higher levels, which are strongly influenced by excitation and ionization from level 2, and hence the optical depths in lines and continua and the strengths of the higher recombination lines.

The light curve of Hα is the least sensitive of the hydrogen lines to our assumptions. The early part of the light curve fits the observations well, but our model underpredicts the observed flux starting at the time of dust formation, ~600 days. There are two straightforward explanations for such a discrepancy. The first is that we overestimate the internal extinction, as discussed above, since the dust optical depth is becoming quite high at later times. The second is that a contribution from delayed recombination in the low-density outer envelope, which we do not model here, is becoming important at later times, as discussed by Kozma & Fransson (1993). Note that Xu et al. (1992) had to introduce an extra ionization source as a free parameter in order to fit the observations of the Hα line. By including two-photon emission, dust grains, and metal opacity in our model, we are now able to explain the Hα light curve without this parameter.

The Hβ light curve is interesting, since it contains a clear feature, a shoulder extending from approximately 400 to 700 days. This feature was predicted by Xu et al. (1992), and it corresponds to the time interval during which Paα is optically thin but Hβ is optically thick, so that most Hβ photons do not escape, but are scattered until a decay to level 3 rather than level 2 occurs, with the Paα photon escaping. This effectively splits the initial Hβ photon into Paα and Hα ("case C recombination"). The splitting process sets in when Paα becomes optically thin, suppressing the Hβ light curve below the general trend from the radioactive decay. As Hβ becomes less and less optically thick, the splitting process becomes negligible ("case B"). The plateau represents the transition from case C to case B. The fact that the shoulder is so clear in the observations suggests that our simple one-zone approximation is not bad, since if the hydrogen emitting region would consist of many regions with individual optical depths, the shoulder would be washed out by the superposition of contributions from the different zones.

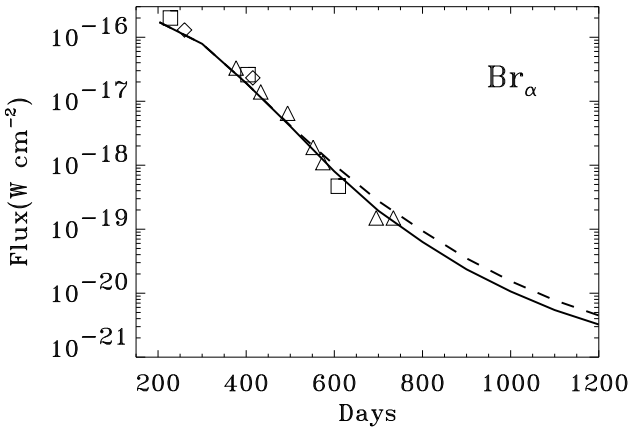


FIG. 8*a*

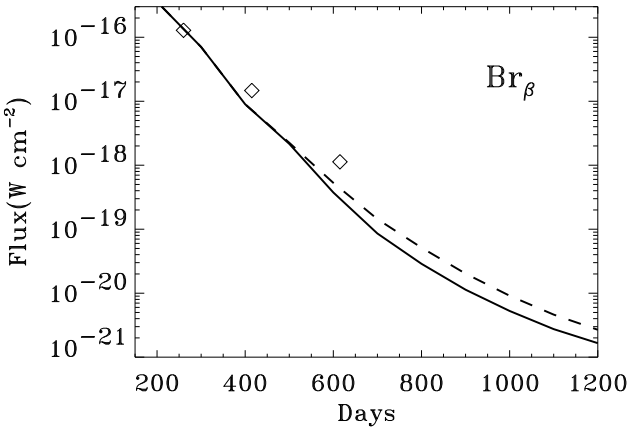


FIG. 8*b*

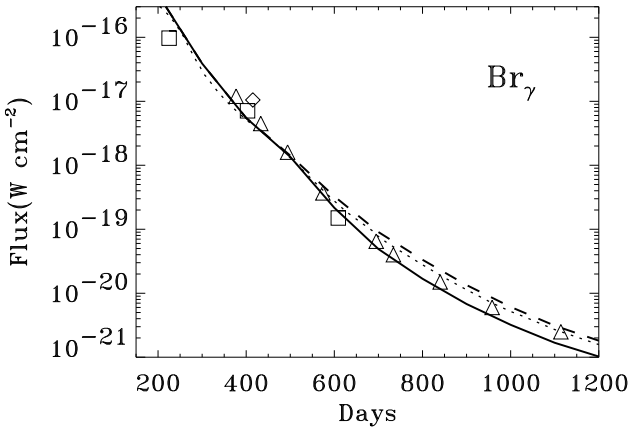


FIG. 8*c*

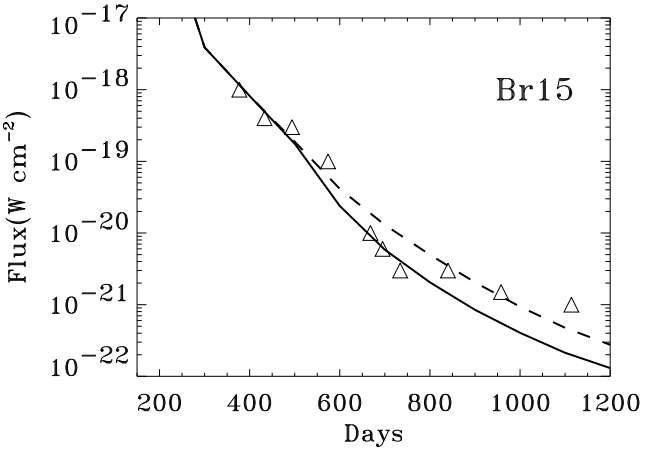


FIG. 8*d*

FIG. 8.—Light curves of Brackett series. *Solid line:* Observable flux; *thick dashed line:* without extinction. (*c*) *Dotted line:* Model with 3 $M_\odot$ of hydrogen. Observations: *diamonds*, Wooden, et al. (1993); *triangles*, Meikle et al. (1993); *squares*, E. Oliva (1994, private communication).

Our results for Hβ do not fit the observed light curve in detail, however. The model results are deficient after dust formation, perhaps because we have overestimated the extinction. The unabsorbed light curve is close to the observed one, but even so a discrepancy remains. Therefore, we suspect that our model is too optically thick. A good fit would result if the plateau would set in and end at slightly earlier times. One way of realizing this situation is to assume a higher value of the metal opacity at Lyα, which decreases the population of level 2 of H, and hence the optical depths. However, this device would cause the fits of the other hydrogen lines to become worse. We also note that using an alternative expression for the continuum destruction probability of Lyα, such as the complete redistribution approximation that we used in our earlier work, can shift the plateau to much earlier times. However, since partial redistribution appears to be a better assumption under the conditions in the supernova envelope (KF), we do not see this as a likely cause of the discrepancy. The dotted and dash-dotted curves in Figure 8*b* show, respectively, how the Hβ light curve would change as a result of changing the continuum opacity by a factor of 10 or of using the continuum destruction probability for complete redistribution.

The Paα and Paβ light curves underpredict the observed flux at early times. The models predict that Paβ goes through a "splitting" phase during the time that case D applies, analogous to the one that Hβ experiences during case C, leading to the structure in the curve between 200 and 500 days. However, the observations display no sign of this behavior. A hint of flattening in the observed light curve between 200 and 300 days suggests that our models become optically thin in the hydrogen transitions too late, consistent with the interpretation that we suggest for Hβ.

The Brackett lines shown in Figure 8 are generally close to the observed light curves. Only for Brβ do we find a larger discrepancy, possibly due to contamination by another line at later times. The excess emission in the Brackett 15 line at late times is almost certainly due to delayed recombination in the low-density outer envelope.

In Figure 8*c*, the Brγ light curve, we have also shown the light curve for a model with a reduced hydrogen mass of 3 $M_\odot$ to illustrate that the hydrogen lines are insensitive to the total hydrogen mass.

8.2.4. *Helium*

Figure 10 shows the He I 1.083 μm and He I 2.058 μm lines. Generally, the model agrees rather well (within a factor of 2) with the observations. The He I 2.058 μm line is somewhat too bright before 500 days, but the discrepancy is

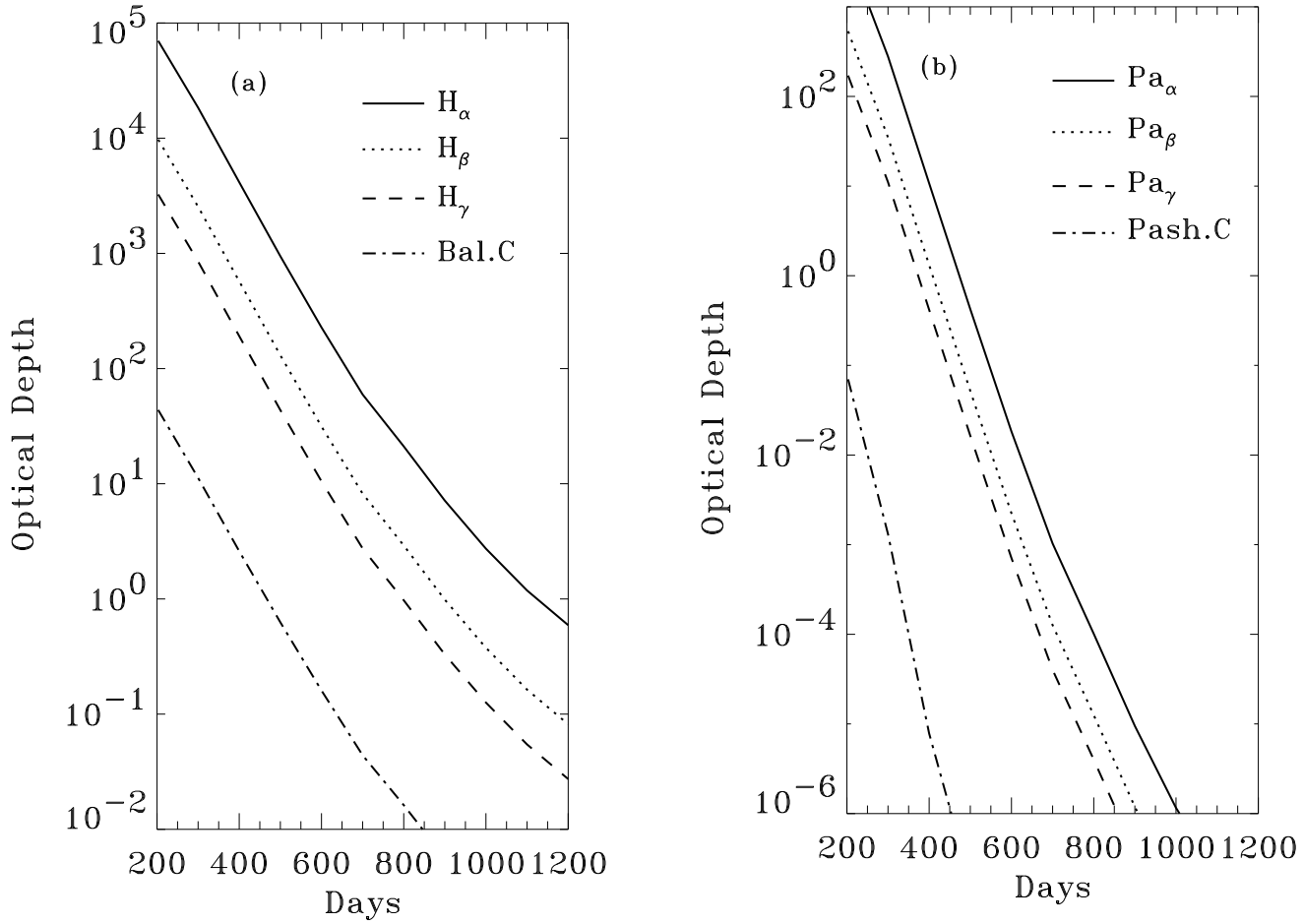


FIG. 9.—Optical depths of hydrogen lines and continua. (*a*) *Solid line:* Hα; *dotted line:* Hβ; *dashed line:* Hγ; *dot-dashed line:* Balmer continuum. (*b*) *Solid line:* Paα; *dotted line:* Paβ; *dashed line:* Paγ; *dot-dashed line:* Paschen continuum.

small compared to the uncertainties in the theory, since the masses of the helium zones contributing to the lines are not tightly constrained by supernova models. Furthermore, as discussed by KF, the choice of the continuum destruction probability for the He I λ584 line (eq. [18]) significantly influences the He I 2.058 μm line strength. A higher continuum destruction probability will increase the $A_{ul}^{\rm eff}$ for the He I λ584 line, and hence it will reduce the branching ratio to the He I 2.058 μm line, suppressing its luminosity. This effect plays a significant role only for $t \lesssim 500$ days. Note

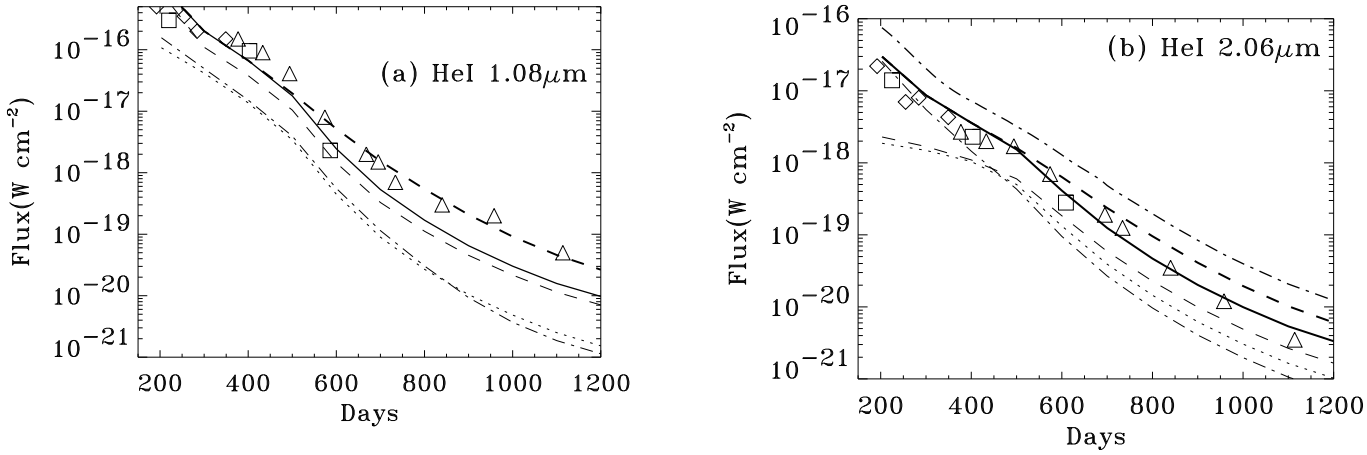


FIG. 10.—Light curves of He I 1.083 μm and He I 2.058 μm. *Thick solid line:* Total emission; *thick dashed line:* total emission without extinction; *dashed line:* hydrogen zone; *dotted line:* helium zone 1; *thin dot-dashed line:* helium zone 2; *thick dot-dashed line:* model with a helium mass of $6\,M_\odot$. Observations of He I 1.083 μm and He I 2.058 μm: *diamonds*, Meikle et al. (1989); *triangles*, Meikle et al. (1993); *squares*, E. Oliva (1994, private communication).

that the choice of metal opacity is not as critical as in the case of hydrogen, since the continuum opacity for He I λ584 is always dominated by hydrogen in the primordial zone and by carbon in the He zone 1.

We may conclude from the shape of the He I 2.058 μm light curves that the mass of the He zone 2 (without extra carbon) cannot be too small; otherwise the light curve before 500 days would be too flat, and the flux at 200 days would be much too low. The light curves from the H and He zone 1 are rather flat owing to the large continuum opacity for the He I λ584 line mentioned in the previous paragraph.

These helium lines were also studied in detail by Li & McCray (1995). Our results differ slightly from theirs in the sense that the fit of the He I 1.083 μm line at early times is significantly better. A common feature is that the ratio of He I 2.058 μm to He I 1.083 μm is slightly too high, although the discrepancy is reduced in the present model. The most likely explanation is that the observed flux of the He I 1.083 μm line also contains contributions from other lines with nearly the same wavelength, notably the [S I] 1.0820 μm line and Paγ (KF).

The flux of the He I 2.058 μm line after 500 days is a good measure of the total helium mass, being roughly proportional to the mass and insensitive to other assumptions. The thick dash-dotted line in Figure 10*b* shows that a model having 6 $M_\odot$ of helium gives a flux that is too large.

8.2.5. *Carbon*

The [C I] $\lambda\lambda$9850, 9826 lines are emitted almost entirely by the helium clumps, mainly from the inner carbon-rich zone where carbon is largely neutral. The carbon in the outer zone is much less abundant than the inner zone and mostly ionized. The predicted and observed fluxes of [C I] $\lambda\lambda$9850, 9826 are shown in Figure 11, where the dotted and dot-dashed curves are the emission from zone 1 and zone 2, respectively, and the solid curve is the total emission. Clearly our model predicts a much stronger line than observed, by as much as a factor of 10 at 400 days. The same result was also found by KF.

We conclude that the actual envelope does not contain as much carbon in carbon-rich He clumps as assumed in our model. Uncertainties in the ionization equilibrium due to the poorly known UV field could perhaps account for a factor of 2 discrepancy, but not for the observed factor of 10. Reducing the mass of the helium clumps by a significant factor could correct for the overly strong [C I] $\lambda\lambda$9850, 9826 lines. Our calculations indicate that a reduction of the carbon abundance in the carbon-rich helium zone to a value 5–10 times smaller than the one obtained from the explosion calculations could also bring agreement with the observations, partly because other cooling processes become more important and partly because the heating rate decreases (see Fig. 3*a*).

8.2.6. *Oxygen*

For oxygen, an important check on our model is the [O I] λ6300 doublet. The predicted flux and observation are shown in Figure 11. For our choice of oxygen abundance, the predicted flux of the [O I] λ6300 doublet varies from 20% to 50% of the observed flux. Since the primordial [O I] λ6300 doublet is completely optically thin, the line ratio of $F(6300)/F(6364)$ should always be 3. This conflicts with the observed line ratio $F(6300)/F(6364) \sim 1{:}1.3$ for $t \lesssim 300$ days, which indicates (Li & McCray 1992) that this emission must come mainly from the optically thick oxygen clumps. To avoid this conflict, we would have to reduce the oxygen abundance in the hydrogen zone to less than half of that inferred by Lundqvist & Fransson (1996) from observations of the SN 1987A ring.

8.3. *Dust Formation and Emission*

As discussed above, the dust formation rate is one of our adjustable parameters, which we calibrate by requiring that the model account for the observed infrared luminosity. The evolution of the dust mass M_d that we infer for the different zones is shown in Figure 12*a*. The total dust masses are $2 \times 10^{-3}\ M_\odot$ in the Fe zone and $1 \times 10^{-3}\ M_\odot$ in the hydrogen and helium zones. Note that these estimated masses do depend on the distribution of dust sizes that we have assumed, and they could be greater if large grains are present. Figure 12*b* shows the total optical depth of the envelope to dust grains at the wavelength of Hα, which reaches a maximum of about 4 between 800 and 1000 days. In Figure 12*c* we present the ratio of the energy deposited in

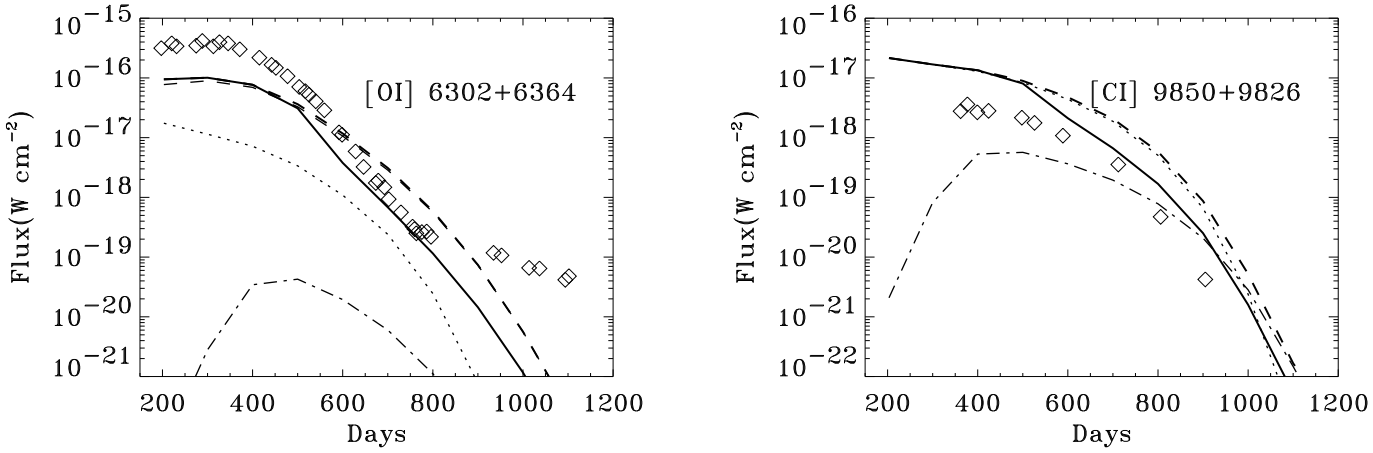


FIG. 11.—Light curves of O I and C I. *Thick solid line:* Total emission; *thick dashed line:* without extinction; *thin dashed line:* from hydrogen zone; *dotted:* helium zone 1; *dot-dashed line:* helium zone 2. Observations of [O I] $\lambda\lambda$6300, 6364: Danziger et al. (1991); observations of [C I] $\lambda\lambda$9850, 9826: Phillips & Williams (1991).

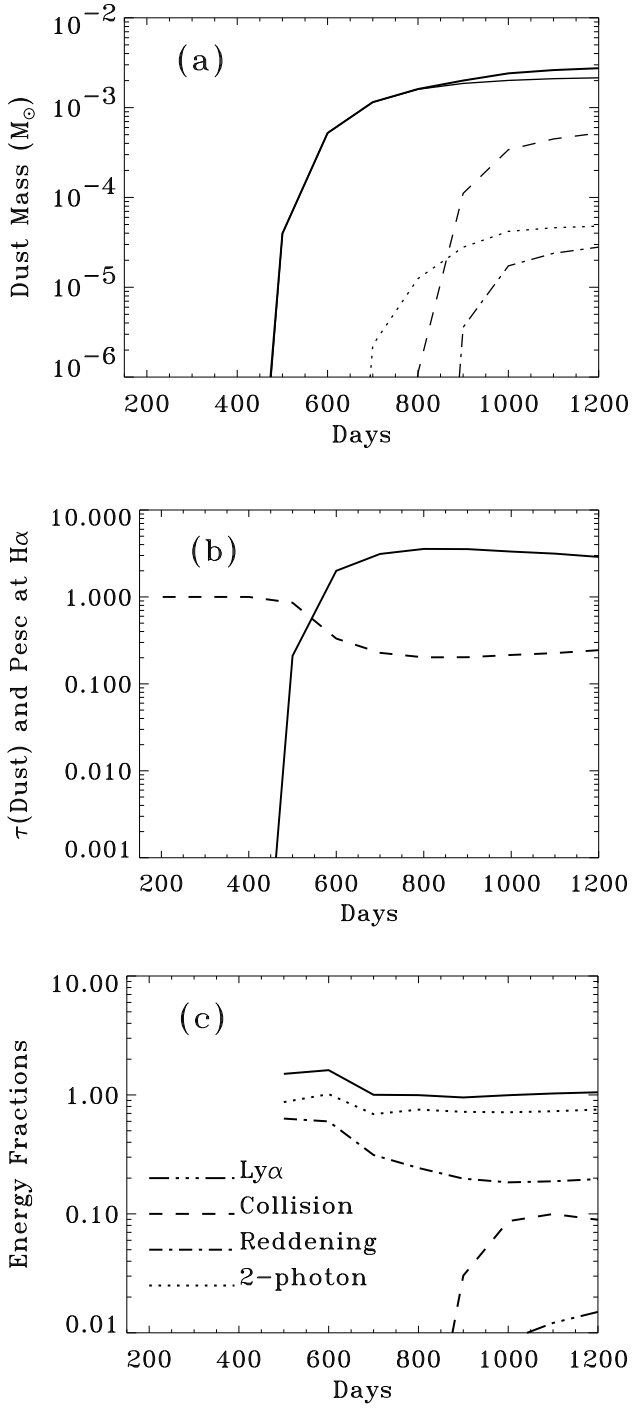


FIG. 12.—Dust grains formed in the envelope of SN 1987A. (*a*) Dust mass required for the standard model. *Thick solid line:* total mass; *thin solid line:* Fe/Co/Ni zone; *dashed line:* H zone; *dotted line:* helium zone 1; *dot-dashed line:* helium zone 2. (*b*) Optical depth of dust grains at the Hα wavelength (*solid line*) and the corresponding volume-average escape probability (*dashed line*). (*c*) Ratios of heating rates of grains to the observed infrared luminosity. *Dashed line:* Collisions with atoms; *dotted line:* absorption of H I and He I two-photon continua; *dot-dashed line:* absorption (reddening) of optical and infrared lines; *three-dot–dashed line:* absorption of Lyα; *solid line:* total heating.

dust grains to the observed dust emission. The dashed curve is the result of collisions with hydrogen atoms, helium atoms, and electrons. The dotted curve is the absorption of H I and He I two- photon continua; the dot-dashed curve is the absorption of all emission lines (reddening); the three-dot–dashed line is the absorption of Lyα; and the solid curve is the sum of these four contributions. At all times considered, the hydrogen two-photon continuum is the main source of heating for the dust grains.

9. DISCUSSION AND SUMMARY

We have determined the temperature and ionization evolution in the envelope of SN 1987A during the nebular phase (from 200 to 1200 days), taking into account all heating, cooling, ionization, and excitation processes that are likely to be important. We then calculated the emission-line light curves of some selected lines, and we find that we can account reasonably well for the observed light curves of H I, He I, Ca II, and Fe II lines, except for Hβ and [Fe II] λ7157.

9.1. *Physical Conditions*

The temperature of the primordial gases is $\sim 6000 \pm 300$ K for $t \lesssim 300$ days, decreases to $\sim 2000 \pm 200$ K at day 800, and then to 1000 ± 200 K after day 1000. The estimated uncertainties are based on calculations of a range of models in which the metal opacity was varied by a factor of 10, the hydrogen mass ranged from 3 to 10 $M_\odot$, and the helium mass from 2 to 6 $M_\odot$. The ionization fraction of hydrogen is $\sim 0.7\%$ at day 200, and it decreases to $\sim 2 \times 10^{-4}$ at day 1200.

The two helium zones have different temperatures. The inner zone (carbon-rich) has a temperature of ~ 5100 K at day 200 and ~ 700 K at day 1200. The outer zone has a temperature of ~ 6000 K at day 200 and ~ 800 K at day 1200. Their ionization fractions are similar, $\sim 1\%$ for $t \lesssim 400$ days, then decreasing to $\lesssim 0.1\%$ at day 1200.

9.2. *Hydrogen and Helium Masses*

From our description of the expected line emission of H and He in § 8 it is clear that accurate mass determinations are not possible because of the dependence of the line fluxes on the metal opacity and radiative transfer effects. In Figure 13 we have plotted the ratio of the He I 2.058 μm and Brγ line fluxes, together with the observations. This ratio should give a direct measurement of relative amounts of hydrogen and helium in the remnant, although it should be kept in

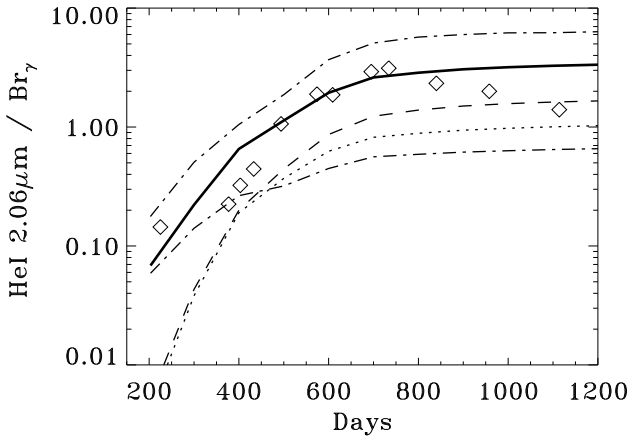


FIG. 13.—Line flux ratio of He I 2.058 μm to H Brγ. *Solid line:* standard model; *dashed line:* from H zone alone; *dotted line:* contribution of helium zone 1 to He I 2.058 μm; *dot-dashed line:* contribution of helium zone 2; *thick dot-dashed line:* model with a hydrogen mass of 3 $M_\odot$. Observations: Meikle et al. (1993) and E. Oliva (1994, private communication).

mind that both fluxes depend on different assumptions, so that this ratio is not more reliable than the individual fluxes. We see that our standard model, which has a somewhat lower helium content than might have been expected (Woosley 1994, 1988), can reproduce this ratio. This ratio is more sensitive to the hydrogen mass than the hydrogen line fluxes themselves. Together with the limits on the helium mass, it gives an indirect limit to the hydrogen mass. This point is illustrated by the dash-dotted line in Figure 13, which represents a model with 3 $M_\odot$ of helium as in the standard model, but with only 3 $M_\odot$ of hydrogen. The fact that the line ratio is too high in this model implies that the hydrogen mass must be significantly greater than the helium mass.

These considerations lead us to the following conclusions:

1. There must be a significant mass of hydrogen in the core ($v < 2500$ km s^{-1}). Models with a hydrogen mass < 4 $M_\odot$ systematically yield a ratio of He I 2.058 μm to Brγ that is too large compared to observations. The upper limits on the hydrogen mass are not tightly constrained; models with up to 10 $M_\odot$ of hydrogen can still give acceptable fits.

2. The upper limit on the helium mass (including the helium zones) is about 5 $M_\odot$, otherwise the He I 2.058 μm line would be too strong at later times. The lower limit is about 2 $M_\odot$.

3. The high continuum opacity for the He I λ584 line in the hydrogen zone (or in the carbon-rich helium zone if the carbon abundance is as high as C:He $\sim 10^{-2}$) suppresses the He I 2.058 μm flux significantly at early times. The slope of the early part of the He I 2.058 μm light curve indicates that some fraction ($\sim$0.5–1.0 $M_\odot$) of the helium must reside in a zone where this continuum opacity is lower, such as the carbon-poor helium zone.

9.3. *Metal Abundances*

Allowing for uncertainties in opacity, dust formation, and masses of the individual composition zones, we can fit most of the observed emission-line light curves reasonably well without adjusting our initial choice of abundances. These were based partly on explosion calculations (for the helium zones), partly on observations of the circumstellar material, and on scaled solar abundances for those elements not otherwise constrained.

The two notable exceptions are the [C I] $\lambda\lambda$9850, 9826 and [O I] λ6300 doublets, both of which are overproduced, and would require a significant deviation from our standard choice of masses and abundances to make the model agree with observation. For the [C I] $\lambda\lambda$9850, 9826 lines, the only solutions appear to be either a significant reduction of the carbon abundance in the carbon-rich helium zone or a much smaller mass for this zone. Most of the [O I] λ6300 emission in our model comes from the hydrogen zone, so we probably do not have as much freedom to change the mass of this zone. A reduction of the hydrogen mass to 3 $M_\odot$, the lower limit metioned above, would reduce the discrepancy significantly, but we consider it more likely that the oxygen abundance is slightly lower than we have assumed.

9.4. *Limitations of the Model*

Although a large amount of detailed atomic physics goes into our model, it should be kept in mind that it represents an extreme simplification of the real supernova envelope. There are two main sources of uncertainty. The first is the crude approximation of the pseudocontinuum metal opacity. Li & McCray (1996) have shown that this problem is solvable in principle, but in practice, performing the necessary Monte Carlo simulations in an iterative time-dependent model would be very time consuming. Furthermore, such simulations would still have to deal somehow with the other main problem of modeling SN 1987A, namely, the unknown geometry. Our assumption of uniform gamma-ray illumination has the advantage of simplicity, but it is obviously an oversimplification. In a different approach, KF have modeled the deposition of gamma-ray energy in the envelope with a geometry in which the zones of different composition remain in concentric shells, as suggested by one-dimensional supernova explosion models. Since observations clearly show that extensive mixing of explosion products has taken place, this geometry is also an oversimplification of the actual situation, and it involves significantly more complexity than our approximation. In the absence of independent knowledge of the geometrical distribution of the different composition zones in the supernova envelope, we do not believe that we would make substantial further progress in understanding the nebular spectrum by attempting to model the gamma-ray and UV/optical photon transport in a complex three-dimensional geometry.

Despite the limitations of the present model, we are gratified to see that our results agree in large part with the observations and with the independent calculations of KF. Evidently, the main results are not very sensitive to the details of the geometry, and we have identified and modeled the main physical processes controlling the thermal evolution and line emission of the hydrogen and helium zones in the inner envelope of SN 1987A.

This work was supported by the National Science Foundation through grant AST 95-29256. Special thanks go to Cecilia Kozma and Claes Fransson for making their preliminary results available to us and for pointing out the important role of the choice of the continuum destruction probability. We also thank the referee, David Hollenbach, for several constructive comments that improved the manuscript.

REFERENCES

Aggarwal, K. M., Berrington, K. A., Burke, P. G., Kingston, A. E., & Pathak, A. 1991, J. Phys. B, 24, 1385
Anders, E., & Grevesse, N. 1989, Geochim. Cosmochim. Acta, 53, 197
Axelrod, T. S. 1980, Ph.D. thesis, Univ. California Santa Cruz
Basko, M. 1994, ApJ, 425, 624
Bakes, E. L. O., & Tielens, A. G. G. M. 1994, ApJ, 427, 822
Burke, J. R., & Hollenbach, D. J. 1983, ApJ, 265, 223
Burrows, A., & Van Riper, K. A. 1995, ApJ, 455, 215
Castor, J. 1970, MNRAS, 149, 111
Chugai, N. N. 1987, Astrophysics (USSR), 26, 53
Colgan S. W. J., & Hollenbach, D. J. 1988, ApJ, 329, L25
Colgan, S. W. J., Haas, M. R., Erickson, E. F., Lord, S. D., & Hollenbach, D. J. 1993, ApJ, 427, 874
Cunto, W., & Mendoza, C. 1993, The Opacity Project Atomic Database, IBM Venezuela Scientific Center Rep. CSC-01-92
Danziger, I. J., Lucy, L. B., Bouchet, P., & Gouiffes, C. 1991, in Supernovae, ed. S. E. Woosley (New York: Springer), 69
Dopita, M. A., & Meatherington, S. J. 1991, ApJ, 377, 480
Draine, B. T. 1995, in ASP Conf. Ser. 80, The Physics of the Interstellar Medium and Intergalactic Medium, ed. A. Ferrara, C. F. McKee, C. Helles, & P. R. Shapiro (San Francisco: ASP)
Draine, B. T., & Lee, H. M. 1984, ApJ, 285, 89

Draine, B. T., & Sutin, B. 1987, ApJ, 320, 803
Drake, G. W. F., Victor, G. A., & Dalgarno, A. 1969, Phys. Rev., 180, 25
Dufour, R. J. 1984, in Structure and Evolution of the Magellanic Clouds, ed. S. Van Den Bergh & K. S. De Boer (Dordrecht: Reidel), 353
Dwek, E., Moseley, S. H., Glaccum, W., Graham, J. R., Loewenstein, R. F., Silverberg, R. F., & Smith, R. K. 1992 ApJ, 389, L21
Erickson, E. F., Haas, M. R., Colgan, S. W. J., Lord, S. D., Burton, M. G., Wolf, J., Hollenbach, D. J., & Werner, M. 1988, ApJ, 330, L39
Fransson, C., & Chevalier, R. A. 1987, ApJ, 329, L25
Fransson, C., Houck, J., & Kozma, C. 1996, in IAU Colloq. 145, Supernovae and Supernova Remnants, ed. R. McCray & Z.-R. Wang (Cambridge: Cambridge Univ. Press), 211
Fuhr, J. R., Martin, G. A., & Wiese, W. L. 1988, J. Phys. Chem. Ref. Data, 17, S4
Haas, M. R., Colgan, S. W. J., Erickson, E. F., Lord, S. D., Burton, M. G., & Hollenbach, D. J. 1990, ApJ, 360, 257
Hummer, D. G. 1968, MNRAS, 138, 73
Hummer, D. G., & Rybicki, G. B. 1985, ApJ, 293, 258
Kozma, C., & Fransson, C. 1992, ApJ, 390, 602
———. 1993, ApJ, 408, L25
———. 1998a, ApJ, in press, 496, 946 (KF)
———. 1998b, ApJ, in press, 497, 431 (KF)
Li, H., & McCray, R. 1992, ApJ, 387, 309
———. 1993, ApJ, 405, 730
———. 1995, ApJ, 441, 821
———. 1996, ApJ, 456, 370
Li, H., McCray, R., & Sunyaev, R. A. 1993, ApJ, 419, 824
Lucy, L. B., Danziger, I. J., Gouiffes, C., & Bouchet, P. 1989, in IAU Colloq. 120, Structure and Dynamics of the Interstellar Medium, ed. G. Tenorio-Tagle, M. Moles, & J. Melnick (Berlin: Springer), 164
Lundqvist, P., & Fransson, C. 1996, ApJ, 464, 924
McCray, R. 1993, ARA&A, 31, 175
———. 1996, in IAU Colloq. 145, Supernovae and Supernova Remnants, ed. R. McCray & Z.-R. Wang (Cambridge: Cambridge Univ. Press), 223
McGregor, P. J. 1988, Proc. Astron. Soc. Australia, 7, 45
Meikle, W. P. S., Allen, D. A., Spyromilio, J., & Varani, G.-F. 1989, MNRAS, 238, 193.
Meikle, W. P. S., Spyromilio, J., Allen, D. A., Varani, G.-F., & Cumming, R. J. 1993, MNRAS, 261, 535
Mihalas, D. 1978, Stellar Atmospheres (New York: Freeman)
Moseley, S. H., Dwek, E., Glaccum, W., Graham, J. R., Loewenstein, R. F., & Silverberg, R. F. 1989, ApJ, 347, 1119
Nussbaumer, H., & Schmutz, W. 1984, A&A, 138, 495
Osterbrock, D. E. 1989, Astrophysics of Gaseous Nebulae and Active Galactic Nuclei (Mill Valley: University Science Books)
Phillips, M. M., Hamuy, M., Heathcote, S. R., Suntzeff, N. B., & Kirhakos, S. 1990, AJ, 99, 1133
Phillips, M. M., & Williams, R. E. 1991, in Supernovae, ed. S. E. Woosley (New York: Springer), 36
Roche, P. F., Aitken, D. K., Smith, C. H., & James, H. D. 1989, Nature, 337, 533
Sawey, P. M. J., & Berrington, K. A. 1993, At. Data Nucl. Data Tables, 55, 81
Sobolev, V. 1957, Soviet Astron., 1, 678
———. 1960, Moving Envelope of Stars (Cambridge, MA: Harvard Univ. Press)
Spyromilio, J., Stathakis, R. A., Cannon, R. D., Waterman, L., Couch, W. J., & Dopita, M. A. 1991, MNRAS, 248, 465
Suntzeff, N. B., Phillips, M. M., Depoy, D. L., Elias, J. H., & Walker, A. R. 1991, AJ, 102, 1118
Swartz, D. A., Harkness, R. P., & Wheeler, J. C. 1987, Nature, 337, 439
Terndrup, D. M., Elias, J. H., Gregory, B., Heathcote, S. R., Phillips, M. M., Suntzeff, N. B., & Williams, R. E. 1988, Proc. Astron. Soc. Australia 7, 412
Wang, L., et al. 1997, ApJ, 466, 998
Wiese, W. L., Smith, M. W., & Glennon, B. M. 1966, Atomic Transition Probabilities, Vol. I (Washington, DC: GPO)
Wiese, W. L., Smith, M. W., & Miles, B. M. 1969, Atomic Transition Probabilities, Vol. II (Washington, DC: GPO)
Wooden, D. H., Rank, D. M., Bregman, J. D., Witteborn, F. C., Tielens, A. G. G. M., Cohen, M., Pinto, P. A., & Axelrod, T. S. 1993, ApJS, 88, 477
Woosley, S. 1988, ApJ, 330, 218
Woosley, S., Pinto, P. A., & Hartmann, D. 1989, ApJ, 346, 395
Xu, Y., & McCray, R. 1991, ApJ, 375, 190
Xu, Y., McCray, R., Oliva, E., & Randich, S. 1992, ApJ, 386, 181